

Durham Research Online

Deposited in DRO:

04 July 2014

Version of attached file:

Accepted Version

Peer-review status of attached file:

Peer-reviewed

Citation for published item:

Watson, F. E. and Mathias, S. A. and Daniels, S. E. and Jones, R. R. and Davies, R. J. and Hedley, B. J. and van Hunen, J. (2014) 'Dynamic modelling of a UK North Sea saline formation for CO₂ sequestration.', *Petroleum geoscience.*, 20 (2). pp. 169-185.

Further information on publisher's website:

<http://dx.doi.org/10.1144/petgeo2012-072>

Publisher's copyright statement:

Accepted for publication in *Petroleum Science* as of 25 February 2014.

Additional information:

Use policy

The full-text may be used and/or reproduced, and given to third parties in any format or medium, without prior permission or charge, for personal research or study, educational, or not-for-profit purposes provided that:

- a full bibliographic reference is made to the original source
- a [link](#) is made to the metadata record in DRO
- the full-text is not changed in any way

The full-text must not be sold in any format or medium without the formal permission of the copyright holders.

Please consult the [full DRO policy](#) for further details.

1 **Dynamic modelling of a UK North Sea saline formation for CO₂** 2 **sequestration**

3
4 Francesca E. Watson, Simon A. Mathias, Susie E. Daniels, Richard R. Jones, Richard J. Davies, Ben J.
5 Hedley, Jeroen van Hunen

6 7 **Abstract**

8 Preliminary dynamic modelling, using TOUGH2/ECO2N, has been carried out to assess the suitability
9 of a site in the UK North Sea for sequestering CO₂. The potential storage site is a previously unused
10 saline formation within the Permian Rotliegend sandstone. Data regarding the site is limited.
11 Therefore, additional input parameters for the model have been taken from the literature and
12 nearby analogues. The sensitivity of the model to a range of parameters has been tested. Results
13 indicate that the site can sustain an injection rate of around 2.5 Mt a⁻¹ of CO₂ for 20 years. The main
14 control on pressure buildup in the model is the permeability of the unit directly beneath the
15 Rotliegend in the location of the proposed storage site. The plume diameter is primarily controlled
16 by the porosity and permeability of the site. A comparison between static, analytical and dynamic
17 modelling highlights the advantages of dynamic modelling for a study such as this. Further data
18 collection and modelling is required to improve predictions of pressure buildup and CO₂ migration.
19 Despite uncertainties in the input data, the use of a full 3D numerical simulation has been extremely
20 useful for identifying and prioritising factors which need further investigation.

21 **Keywords:**

22 Carbon sequestration, CO₂, dynamic modelling, UK North Sea, saline formation, greenhouse gas,
23 global warming, climate change

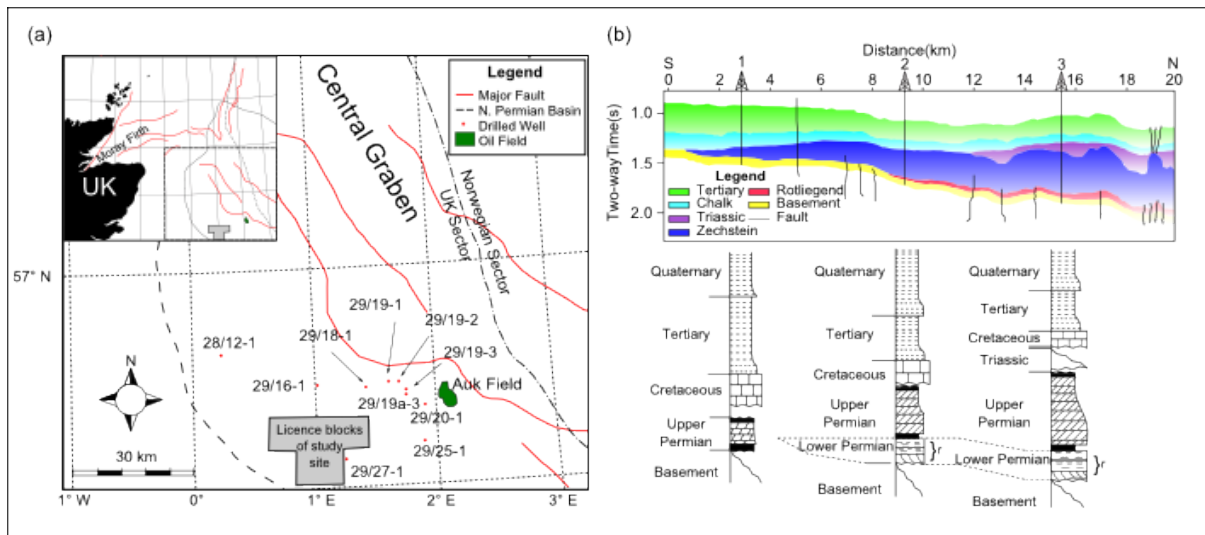
24
25
26 Carbon sequestration has been proposed as a method of keeping atmospheric greenhouse gas
27 emissions at an acceptable level (Pacala and Socolow 2004). Deep saline formations are one possible
28 storage option for CO₂ as they contain large volumes of pore space and are regionally extensive
29 (IPCC 2005). One of the advantages of using previously unused saline formations for CO₂ storage is
30 the fact that they may have a reduced well density compared with oil or gas fields. Therefore, the
31 number of man made leakage pathways is reduced. This is also a disadvantage as it means that there
32 is limited data available about the formation for site-scale characterisation.

33 The EU directive (European Union 2009) requires the screening of a range of sites in order to identify
34 those which are promising for CO₂ storage. Potential storage sites, chosen from preliminary
35 screening, then need to be fully characterised using static and dynamic computer simulations which
36 should demonstrate storage capacity, pressure buildup and CO₂ migration pathways. A site can only

37 be used for CO₂ storage if the site characterisation indicates that the risk of CO₂ leakage is
38 insignificant and that there are no significant risks to human health or the environment.

39 This paper describes a preliminary site characterisation, undertaken for a deep saline formation in
40 the North Sea, using a very limited dataset. This comes after the regional screening stage but is prior
41 to the full site characterisation stage of the CO₂ storage workflow described above. The aim of the
42 work is to build a dynamic model with which to assess the potential for CO₂ storage at the proposed
43 site and to identify further data which will be needed before a thorough site assessment can be
44 carried out.

45 The site being considered for CO₂ storage is located in the Central North Sea (Fig. 1(a)). It is 50 km
46 west of the Central Graben and 70km north of the Mid North Sea High, on the south western edge of
47 the Northern Permian Basin. This is approximately 200 km North East of the UK Teesside industrial
48 processing region which could provide the source of CO₂. The potential storage formation is the
49 Permian Rotliegend Sandstone with the Permian Zechstein Salt providing the cap rock (Glennie
50 1983).



51
52 **Fig. 1. (a)** Location map of the study site showing wells logs used in this study. **(b)** Regional structure
53 and stratigraphy based on regional seismic line. Schematic wells show lateral variations in unit
54 thickness. The reservoir interval is denoted (r). After Hedley et al. (2013).

55 The intended preliminary trap within the Rotliegend is referred to hereafter as the CCC Prospect. A
56 2D seismic survey carried out over the proposed storage site shows that the CCC Prospect consists of
57 a series of interconnected four-way dip closures. It is known that the Rotliegend pinches out to the
58 south west of the site about 30 km away from the CCC Prospect (Fig. 1(b)). As the pinchout is updip
59 from the CCC Prospect it could form a secondary trap in the event of CO₂ escaping from the CCC site.

60 **CO₂ storage in saline formations in the UK North Sea**

61 In order to meet emissions reductions targets the UK may need to store between 2 and 5 billion
62 tonnes of CO₂ before 2050. The Department for Energy and Climate Change estimated that the UK
63 has the potential to store 60 billion tonnes of CO₂ within saline formations in the UK North Sea and
64 the East Irish Sea (DECC 2012). However, this storage capacity is not well understood and requires
65 further investigation before storage operations can begin.

66 Formations within the North Sea have proven ability to store CO₂ both in natural accumulations
67 (Yielding *et al.* 2011) and as part of a large scale carbon sequestration project (Chadwick *et al.*
68 2009b; Boait *et al.* 2012). Currently there is no injection of CO₂ for storage purposes within the UK
69 North Sea.

70 Most previously published work regarding CO₂ storage in specific saline formations in the UK North
71 Sea has been associated with the Triassic Bunter Sandstone Formation, within the Southern North
72 Sea. Bentham *et al.* (2006) estimated the total storage capacity for several structures within the
73 Bunter Sandstone based on their pore volume, CO₂ density at reservoir conditions and a factor
74 representing the proportion of pore space likely to be filled with CO₂. This factor was derived
75 from a numerical model of a planned CO₂ injection into the Esmond field in the Bunter Sandstone.
76 These estimates were mostly constrained by plume geometry and did not include the potentially
77 limiting effect of pressure buildup on CO₂ injection.

78 Heinemann *et al.* (2012) estimated the dynamic storage capacity of the Bunter Sandstone by
79 approximating it as a series of identical unit cells each containing an injection well at its centre. The
80 minimum allowable well spacing was determined by finding the minimum cell size where the
81 pressure increase due to injection stayed below some maximum pressure threshold. Estimates
82 calculated in this way, which include the impact of pressure buildup on injection, were 2 – 4 times
83 smaller than the static estimates given by Bentham *et al.* (2006). Noy *et al.* (2012) modelled a 113
84 km x 160 km portion of the Bunter Sandstone and estimate that 15 – 20 Mt a⁻¹ could be stored in it
85 over a 50 year period.

86 As part of the CASSEM (CO₂ Aquifer Storage Site Evaluation and Monitoring) project two onshore
87 analogues for potential offshore CO₂ storage sites were modelled (Jin *et al.* 2010). The analogues
88 chosen were the Kinniswood and Knox Pulpit Formations, in the east of Scotland and the Triassic
89 Sherwood Sandstone in the east of England, the second of which is very similar to the Bunter
90 Sandstone. The aim of the CASSEM project was to consider and refine the methods used for site
91 characterisation as opposed to investigating the storage potential of any particular sites. However,
92 they calculated storage efficiencies (the maximum volume of CO₂ stored divided by the total pore
93 volume of the storage site) for the two sites at between 0.46 % and 2.75 %. These efficiencies led to
94 storage capacity estimates of 800 Mt and 2300 Mt which indicate the potential for CO₂ storage at
95 similar sites in the UK North Sea.

96 Our work investigates the potential pressure buildup and plume migration at a specific, field scale
97 site within a larger, regional scale aquifer, in the UK North Sea. The main objective of the study is to
98 determine if the site is generally capable of storing the desired amount of CO₂ without causing an
99 unsustainable increase in pressure or leading to migration of CO₂ over large distances. This
100 preliminary site investigation will provide information on the feasibility of storing CO₂ at this site and
101 the further data which will be needed to carry out a thorough site investigation. We also describe
102 the methodology used to build a dynamic model for a site with little existing, direct data. The
103 modelling choices made and the reasons behind them are given, providing a useful reference for
104 building similar models in the future.

105 **Geological Background**

106 After the Carboniferous Variscan Orogeny, north – south extension and thermal subsidence in the
107 North Sea during the Permian formed the Northern and Southern Permian Basins. They are
108 separated by the Mid North Sea High. Rotliegend Sandstone was deposited into the Permian Basins
109 and into the much smaller Moray Firth Basin. In the Late Permian, rifting in the Northern North Sea
110 and rising sea levels led to the opening up of a seaway which allowed the Zechstein Marine
111 Transgression to occur, forming the Permian Zechstein Salt (Taylor 1998). Subsequent east – west
112 extension led to the formation of the Central and Viking Grabens which cross cut the Permian Basins.

113 **Proposed storage site**

114 The CCC prospect is located on the edge of the Northern Permian Basin within the Rotliegend and
115 consists of three interconnected four-way dip closures which can be seen in the depth converted
116 seismic data. It covers an area of 26.5 km² and is approximately 2600 m below sea level. The
117 thickness of the storage formation at this point is uncertain as it is not possible to identify the base
118 of the formation on the seismic data. Also, no wells penetrate the base of the Rotliegend in this area.
119 It is estimated that beneath the CCC prospect the Rotliegend is 100 – 300 m thick.

120 The Rotliegend in our study area consists of Auk Formation deposits. The Auk Formation covers a
121 large part of the Northern Permian Basin and is composed solely of sedimentary rocks. It was
122 deposited at a time when the climate of the region was arid desert. Aeolian sandstones dominate
123 the sequence with some fluvial and lacustrine facies also present. The prominent wind direction at
124 the time was most likely from the north west (Glennie 1983; Glennie *et al.* 2003).

125 The Rotliegend forms a hydrocarbon reservoir in the nearby Auk field (Fig. 1(a)). Several studies have
126 characterised the Rotliegend at the Auk field using core data (Heward 1991; Trewin *et al.* 2003).
127 Heward (1991) divided the reservoir into several layers with different porosities and permeabilities
128 according to the facies present within them. It is possible that this facies variation is also present in
129 the CCC prospect.

130 Core data from wells near the storage site indicate that the lithology of the Rotliegend at the site is
131 most likely similar to the fluvial and dune facies seen in the Auk field.

132 **Caprock**

133 The Zechstein Marine Transgression occurred during the late Permian and covered both the
134 Northern and Southern Permian basins. Changes in sea level due to periodic glaciation and retreat
135 led to several cycles of transgression and subsequent evaporation of the Zechstein Sea. This
136 sequence of transgression and evaporation led to the deposition of a thick evaporite layer in the
137 centre of the basin, predominantly composed of halite. A higher proportion of carbonates and
138 anhydrite exists at the shallower edges of the basin. Some dolomitisation has occurred within the
139 basin as a whole. Salt tectonics are common in the thicker, halite sections of the basin (Taylor 1998).
140 This is when salt layers deform ductilely due the relatively low density salt being overlain by
141 relatively high density strata. The movement of salt can disrupt the overlying strata potentially
142 creating pathways for fluid leakage.

143 It is not possible to discriminate between the different Zechstein facies by interpretation of the
144 seismic data. Dolomite rafts can have high porosity but it is thought, from seismic and well data, that
145 there is > 800 m thickness of halite above the site which will provide a competent caprock with

146 sufficient sealing capacity. Salt tectonics can clearly be seen in the seismic data to the north east of
147 the proposed storage site.

148 **Base Unit**

149 The Rotliegend in our study area is thought to lie unconformably upon Devonian Old Red Sandstone.
150 This is not known for certain as no wells have penetrated the base of the Rotliegend in this area,
151 however the Rotliegend is directly above Devonian strata in the Auk field (Trewin *et al.* 2003) and in
152 the Argyll and Innes fields to the east of the storage site (Heward *et al.* 2003). Alternatively the
153 Rotliegend of the storage site could lie on top of Carboniferous strata. However, it is possible that
154 both the Devonian Old Red Sandstone and Carboniferous rocks in the area have similar porosity and
155 permeability characteristics to the Rotliegend Sandstone.

156 **Modelling**

157 The model has been built to satisfy in part the requirements of the EU Directive (European Union
158 2009), for characterisation of the dynamic behaviour of injected CO₂ in a potential storage site. At
159 present the available input data is not sufficient to provide a complete site characterisation which
160 assesses all aspects required by the EU Directive. The main parameters investigated using this model
161 are the storage capacity of the intended trap, pressure buildup within the storage site and the
162 migration of the CO₂ plume.

163 A choice of modelling methods for site characterisation is available. The simplest of these are
164 analytical methods which provide analytical solutions for one or two model variables such as storage
165 capacity (Zhou *et al.*, 2008), pressure buildup with CO₂ injection (Mathias *et al.*, 2008; Zhou *et al.*
166 2008; Mathias *et al.* 2011), or the radius of the CO₂ plume (Nordbotten *et al.* 2005). These methods
167 are useful as they provide a quick assessment of certain characteristics of a site. However, they
168 require some simplifying assumptions to be made. A common limitation of analytical models is that
169 they are unable to account for heterogeneity in either formation properties or model geometry. As
170 we have access to stratigraphic relief data, in the form of an interpreted seismic layer, we can better
171 model storage capacity, CO₂ migration and pressure buildup specific to our site using a 3D numerical
172 model which incorporates the geometry data.

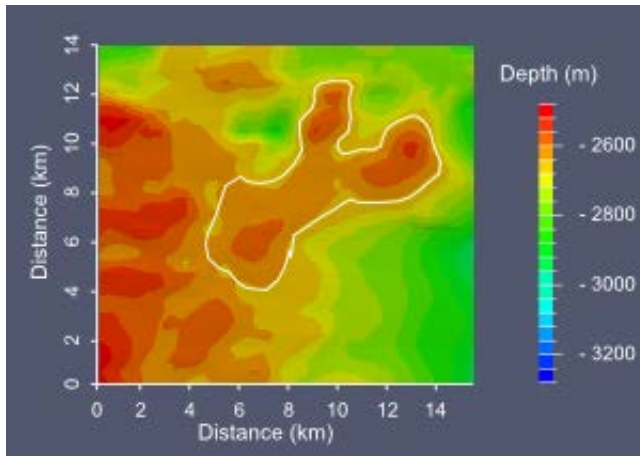
173 3D numerical modelling can be undertaken using several different methods. One potential option is
174 to use streamline based models (Obi and Blunt 2006; Qi *et al.* 2009). Here the model domain is split
175 into small grid blocks and a finite difference approximation is used to calculate pressure in each grid
176 block. The pressure field is then used to trace streamlines which show the fluid flow paths within the
177 model. Flow equations are solved in one dimension, along the streamline, for several timesteps to
178 show the migration of different phase saturations within the storage site. After a certain global
179 timestep size the average saturation of each grid block is calculated from the saturation of the
180 streamlines running through it, the pressure field is updated and the locations of the streamlines are
181 retraced. The whole process is then repeated. This method is computationally efficient as the flow
182 equations are only solved in one dimension, along the streamlines. Also, fewer time consuming
183 pressure calculations have to be carried out. However, streamline simulation is only suitable for
184 modelling systems where the pressure, and therefore the location of the streamlines, does not
185 change much during the relatively large pressure timesteps. As our model involves CO₂ injection
186 with no accompanying production, the pressure change in the system is quite large. Consequently,
187 streamline simulations may not be suitable in this context.

188 Another possible option is to use a vertical equilibrium model (Gasda *et al.* 2009; Gasda *et al.* 2011;
189 Nilsen *et al.* 2011). In this method the model domain is discretised in the horizontal direction but
190 only contains one layer in the vertical direction. The fluids in each cell are assumed to be in a
191 gravitationally stable configuration (vertical equilibrium), therefore no flow in the vertical direction is
192 modelled. Horizontal flow in the model is solved-for using Darcy's law. The height of the interface
193 between fluid phases (CO₂, CO₂ saturated brine, brine) in each cell can then be found, using an
194 analytical solution based on the phase saturations. This method is more computationally efficient
195 than a full three dimensional model as the flow equations are only solved in two dimensions. It
196 allows the horizontal plume spread and the segregation between the different fluid phases to be
197 modelled. However, the assumption that the storage site is in vertical equilibrium means that it is
198 not possible to account for heterogeneity and anisotropy in the vertical direction. Consequently, a
199 vertical equilibrium model is unsuitable for assessing effects associated with layering within
200 formations, such as those potentially present within the Rotliegend.

201 In this study, we consider a more conventional 3D, regular, grid based model which uses an
202 integrated finite difference method to solve the flow and transport equations (Narasimhan &
203 Witherspoon 1976). This is more computationally expensive than other methods as it requires the
204 model to be discretised into a three dimensional grid and therefore the equations have to be solved
205 for more gridblocks at each timestep. However, the chosen method will enable us to better model
206 the pressure increase during the injection period and to include vertical anisotropy in the form of
207 anisotropic permeability and layering within the model.

208 Specifically, modelling has been performed using TOUGH2-MP (Zhang *et al.* 2008), the parallel
209 version of the TOUGH2 numerical code for modelling multiphase flow in porous media (Pruess *et al.*
210 1999). It has been used in conjunction with the ECO2N equation of state module (Pruess 2005),
211 which models mixtures of H₂O-CO₂-NaCl and has been designed specifically to represent conditions
212 applicable to CO₂ storage in saline aquifers. Code comparison studies (Pruess *et al.* 2004) have
213 shown TOUGH2 to be a robust code, capable of modelling complex systems relating to geological
214 storage of CO₂. It is widely used for CO₂ storage simulations (e.g. Chadwick *et al.* 2009a; Doughty
215 2010; Chasset *et al.* 2011).

216 The model covers an area of about 15.75 km by 14.25 km. This encompasses the CCC Prospect but
217 does not extend to the stratigraphic pinchout of the Rotliegend which could form a secondary trap in
218 the event of CO₂ escaping laterally from the CCC Prospect. In the interest of reducing the
219 computational cost of modelling it was decided at this early stage to only model the CCC Prospect
220 and the area immediately surrounding it.



221

222 **Fig. 2.** Depth map of top of the model. White line indicates outline of CCC Prospect.

223 The model is rectangular in area. The base of the Rotliegend layer cannot be distinguished in the
 224 seismic data. A formation thickness of 320 m has been chosen for the base case model. The relief of
 225 the top surface of the model has been interpolated from the depth converted seismic surface of the
 226 top of the Rotliegend (Fig. 2). As the base of the Rotliegend cannot be seen in the seismic data, the
 227 base of the model has been given the same relief as the top of the model.

228 The available seismic data is old and was interpreted using only sparse coverage of well data picks.
 229 This is often the case for CCS modelling studies of previously unused sites (e.g. Noy *et al.* 2012;
 230 Schäfer *et al.* 2012). Seismic data must be integrated with well data to provide a reasonable estimate
 231 of reservoir depth and the thickness of layers within the reservoir. Large uncertainties can be
 232 introduced into the data when well data is sparse and well locations are far from the storage site. To
 233 address this issue we have varied reservoir thickness in one of the model runs. Other dynamic
 234 modelling studies of storage sites within saline formations have used models with flat top and
 235 bottom surfaces (Hovorka *et al.* 2004; Chasset *et al.* 2011). This is due either to a lack of significant
 236 undulation in the surfaces of the modelled units or a lack of seismic data over the modelled site. To
 237 assess the impact of using a model with flat surfaces we have run some simulations with flat top and
 238 bottom surfaces.

239 The horizontal resolution of the model is 5 m around the injection well increasing to 500m at the
 240 edges of the model. To accurately model injection well pressure a very fine horizontal grid resolution
 241 (~ 5 mm) is needed around the injection well (Mathias *et al.* 2011). As the purpose of our model is to
 242 look at the overall capacity of the storage site to store injected CO₂ it was not deemed necessary at
 243 this stage to carry out detailed modelling of injection pressures. Therefore, a larger grid resolution
 244 near the well bore has been chosen in order to increase the computational efficiency of simulations.
 245 This approach of having a relatively large injection cell is taken by several studies investigating field
 246 scale effects of CO₂ injection, particularly for models using fully 3D rectangular grids (Doughty 2010;
 247 Noy *et al.* 2012). Yamamoto *et al.* (2009) used a Voronoi mesh which allowed them to have very fine
 248 grid resolution around their modelled injection wells. However, in their study it was important to
 249 model the effects of several closely spaced injection wells and the corresponding brine migration
 250 caused by the pressure increase around the wells. This is not the case in our work.

251 Vertical resolution is 1 m for the first 10 m below the caprock. Beneath the top 10 m of the model
252 the vertical resolution is 10 m. Yamamoto & Doughty (2011) showed that a coarse vertical grid
253 resolution reduced the maximum radial plume extent at the top of their model, particularly when
254 the injection rate was low (0.1 Mt/a). The injection rate in our models is much higher than this.
255 However, the grid resolution has been increased at the top of the model in order to better capture
256 the plume spread at the top of the storage site.

257 The total number of gridblocks in the base case model is 350714 (94 x 91 x 41).

258 **Initial and boundary conditions**

259 The initial conditions used in the models have been informed by well data and literature data.
260 Where possible, direct data from the Rotliegend formation close to the CCC Prospect have been
261 used. Literature observations regarding nearby analogues and rocks with similar lithologies have
262 been used in preference to more general observations. Empirical observations from the literature
263 have been given priority over theoretical relationships.

264 Pressure information is available from a pressure study undertaken at the site using nearby well data
265 and published information. The site is thought to be slightly overpressured compared to the
266 hydrostatic pressure gradient. Pressure at the top of the site is ~ 33 MPa. The fracture pressure of
267 the Zechstein caprock is estimated to be 47 MPa. In our models pressure has been set at 33 MPa at a
268 depth of 2600 m and a hydrostatic gradient has been allowed to equilibrate.

269 A temperature of approximately 90°C, taken from nearby well logs, has been chosen as the
270 formation temperature at 2600 m depth. A geothermal gradient of 30 °C/km has then been applied
271 to the model. This is a reasonable value for the geothermal gradient in the area of the storage site
272 (Cornford 1990).

273 No direct data is available about existing fluids within the formation. We have assumed that the
274 storage site is initially filled with brine. A salinity of 10.5 % has been used similar to the salinity of
275 formation fluids in the Auk field (Trewin *et al.* 2003). The effect of salt precipitation due to formation
276 dry-out near the injection well (Kim *et al.* 2012) has not been looked at. This effect has implications
277 for injection pressures but has not been included as we are not carrying out detailed modelling of
278 formation injectivity.

279 Appropriate boundary conditions are required to model pressure buildup and fluid migration
280 accurately. The thickness of the salt (up to 1 km) and its low permeability mean it is unlikely that CO₂
281 will leak into the caprock, unless the fracture pressure is exceeded. Therefore a no flow boundary
282 condition has been implemented at the top of the model. The assumption of a no flow boundary at
283 the top seal of the model is frequently used to represent the boundary between a relatively high
284 permeability formation and an extensive, low permeability caprock (Doughty 2007; Hazignatiou *et al.*
285 *al.* 2011). Noy *et al.* (2012) show that reducing the permeability of the caprock leads to an increase
286 in the pressure footprint of the plume. Using a no flow boundary condition instead of modelling the
287 caprock essentially reduces the permeability of the caprock to zero, thus allowing a conservative
288 pressure estimate to be made. The advantage of not modelling the caprock explicitly is a reduction
289 in model complexity and associated computation time.

290 The pressure study of the site suggests that the storage formation is not compartmentalised. To
 291 reflect this, an open boundary condition (constant pressure) has been imposed at the lateral edges
 292 of the model. The nature of the unit beneath the storage site is unknown although it is suspected to
 293 be Devonian Sandstone, similar in nature to the Rotliegend Sandstone. If this is the case, the bottom
 294 boundary will probably allow flow across it and should therefore be modelled as an open boundary.
 295 Sensitivities have been run with closed base boundaries to look at the extreme case of a very low
 296 permeability unit underlying the storage site.

297 **Input parameters**

298 Values for input parameters used for modelling are shown in Table 1.

299

300

	<u>Base case</u>	<u>Ranges modelled</u>
Pressure	33 MPa	-
Temperature	90°C	-
Salinity	10.5 %	-
Porosity	0.19	0.10 – 0.27
Permeability	28 mD (2.76E-14 m ²)	21 – 33 mD (2.07E-14 m ² – 3.26E-14 m ²)
kv/kh	0.1	-
Pore compressibility	1.05E-09 Pa ⁻¹ *	8.73E-10 Pa ⁻¹ – 1.05E-09 Pa ⁻¹
Relative permeability	Function to fit Viking 2 data†	-
Capillary pressure	Function to fit Viking 2 data†	-
Isothermal	Yes	-
Diffusion	No	-
Reservoir thickness	320 m	120 m – 320 m
Injection interval	40 m	40 m – 70 m
Injection rate	2.5 Mt a ⁻¹	-
Simulation length	20 yrs	Post injection – 100 yrs

301 **Table 1.** Model input parameters. * From Jalalh (2006). † From Bennion and Bachu (2006)

302 Porosity and permeability data can either be measured directly from cores or be calculated from
 303 borehole data. There are various ways of calculating porosity and permeability depending on the
 304 data available. Several authors have used depth / porosity correlations and then porosity /
 305 permeability correlations of surrounding units to calculate porosity and permeability of the modelled
 306 units, based on their depth (Eigestad *et al.* 2009; Hazignatiou *et al.* 2011). This has allowed them to
 307 calculate porosity and permeability for areas where no direct porosity and permeability
 308 measurements are available.

309 In our case, porosity values for the Rotliegend are representative values taken from sonic logs of
 310 nearby wells and the literature, and are in the range 10 – 27 % with the most likely value being ~19
 311 % (Selley 1978). Porosity values from the sonic logs were calculated using the equation given by

312 Wyllie et al. (1958). No correction was made for clay content as the part of the Rotliegend
313 penetrated by the logs consists of relatively clean quartz arenite.

314 Horizontal permeability values (k_h) have been taken from core flood data of Rotliegend samples
315 from nearby wells. Permeabilities range from 21 mD ($2.07E-14 \text{ m}^2$) for the finely laminated facies, to
316 33 mD ($3.26E-14 \text{ m}^2$) for the massive sand facies, with 28 mD ($2.76E-14 \text{ m}^2$) for the diffuse laminated
317 facies, taken as the most likely case. The ratio of vertical to horizontal permeability (k_v/k_h) has been
318 chosen as 0.1. A k_v/k_h of 0.1 is similar to values chosen in several studies to represent the fact that
319 permeabilities in siliciclastic rocks are generally greater parallel to the bedding planes (e.g. Ghomian
320 *et al.* 2008; Doughty 2010). The presence of clays within the reservoir would reduce this
321 permeability ratio (Ringrose et al. (2005)) however core data indicates that clay content within the
322 Rotliegend near the CCC Prospect is negligible. Pore compressibility has been estimated using a
323 correlation by (Jalalh 2006) which was calculated in the laboratory and relates porosity and pore
324 compressibility in sandstones.

325 Relative permeability and capillary pressure data have come from the laboratory studies on the
326 Viking 2 sandstone by (Bennion & Bachu 2006). Viking 2 sandstone was chosen as it has similar
327 porosity and permeability values to the estimated values for Rotliegend at our site. The effect of
328 hysteresis, where the multiphase flow properties of the pore space are history dependent, has not
329 been included in our model. Including hysteresis would lead to an increase in residually trapped CO_2
330 and a reduction in the amount of mobile CO_2 which is able to move through the formation (Doughty
331 2007). Consequently CO_2 mobility in our models is at its upper limit, providing a maximum estimate
332 of plume spread.

333 Temperature change through time and dissolution of CO_2 into the brine have not been modelled.
334 Modelling temperature changes can be important when considering the effect of Joule-Thomson
335 cooling (Oldenburg 2007; Mathias *et al.* 2010). This is where CO_2 cools as it undergoes rapid
336 expansion due to a large drop in pressure. This could be the case for injection into a depleted oil or
337 gas reservoir which is at a low pressure but is unlikely to be as important for injection into an aquifer
338 at a pressure similar to that of the injected supercritical CO_2 . Dissolution of CO_2 into the resident
339 brine is an important trapping mechanism. However, in the interest of computational efficiency we
340 have chosen not to model dissolution as the effect of dissolution is relatively small during the early
341 stages of CO_2 injection. Prior to the onset of convection, CO_2 can only dissolve in residually trapped
342 brine which is in contact with free-phase CO_2 . The amount of CO_2 which can dissolve is controlled by
343 the solubility limit of CO_2 in the brine. CO_2 solubility limit in brine, which is dependent on pressure
344 and temperature conditions, can be calculated using the equation of state provided by Spycher and
345 Pruess (2005). Assuming a residual brine saturation of 0.423 (i.e., the Viking 2 core) at 33 MPa and
346 90°C , the amount of CO_2 expected to dissolve in residually trapped brine would represent around
347 3.7% of the total mass of injected CO_2 .

348 The model injection point is located just off crest of the largest dome in the CCC structure. For
349 operational purposes it would be best to inject CO_2 down dip from the structure to be filled.
350 Buoyancy would then transport the CO_2 to the desired location, allowing more of the reservoir to be
351 swept by the CO_2 and therefore increasing residual trapping. In our preliminary model it was
352 decided to locate the injection point much closer to the top of the structure in order to demonstrate

353 containment within the CCC Prospect. This ensures that all the modelled migration of CO₂ is within
354 the CCC Prospect, at least at the beginning of the simulation.

355 Injection has been carried out from a vertical well at a rate of approximately 2.5 Mt a⁻¹ for 20 years.
356 The completion interval varies from 40 m to 70 m. This interval is purposefully small to allow a more
357 conservative estimate to be made of pressure and CO₂ saturation around the injection point. Post
358 injection modelling for most models has been carried out for up to 100 years. Convergence issues,
359 particularly with the layered models meant this was not possible for all models.

360 Input parameters for most of the models are uniform throughout the model domain. Some
361 heterogeneous models were run, where differing permeability and porosity values were assigned to
362 layers within the model. However, no allowance was made in any of the models for lateral
363 heterogeneity in the storage site. This is due to a lack of data describing lateral heterogeneity within
364 the site.

365 **Results**

366 **Base Case**

367

<u>Model</u>	<u>s01a</u>	<u>s01a5</u>	<u>s01b</u>	<u>s01b4</u>	<u>s01c</u>	<u>s01c2</u>	<u>s01d</u>	<u>s01e</u>	<u>s01f</u>	<u>s02a</u>	<u>s02a2</u>	<u>s02a3</u>	<u>s02a4</u>	<u>s03a</u>	<u>s04f</u>	<u>s07a</u>
<u>Permeability</u> Minimum – Min Most likely – ML Maximum – Max	ML	ML	Min	Min	Max	Max	ML	ML	ML	ML	ML	Min	Max	ML	ML	ML
<u>Porosity</u> Minimum – Min Most likely – ML Maximum – Max	ML	Max	Min	ML	Max	ML	ML	ML	ML	ML	ML	ML	ML	ML	ML	ML
<u>Thickness</u> 320 m 120 m	320 m	320 m	320 m	320 m	320 m	320 m	320 m	320 m	320 m	320 m	320 m	320 m	320 m	320 m	120 m	320 m
<u>Layers</u> No Yes	No	No	No	No	No	No	No	No	No	Yes	Yes	Yes	Yes	No	No	Yes
<u>Base Boundary</u> Open Closed	Open	Open	Open	Open	Open	Open	Closed	Open	Closed	Closed	Open	Open	Open	Open	Closed	Open
<u>Lateral boundaries</u> Open Closed	Open	Open	Open	Open	Open	Open	Open	Closed	Closed	Closed	Open	Open	Open	Open	Closed	Open
<u>Topography</u> Yes No	Yes	Yes	Yes	Yes	Yes	Yes	Yes	Yes	Yes	Yes	Yes	Yes	Yes	No	Yes	No
<u>Max. Pressure Increase* 20 yrs</u> (MPa)	1.50	1.52	1.62	1.68	1.36	1.36	2.92	1.50	5.34	3.76	0.68	1.97	0.58	1.49	13.53	0.64
<u>Max. Pressure Increase* 120 yrs</u> (MPa)	0.25	-	0.29	0.26	0.23	-	0.26	0.25	3.17	-	-	-	-	0.19	7.76	-
<u>Plume diameter[†] 20 yrs</u> (km)	1740	1195	2345	1351	1345	1842	1934	1740	1745	1351	2145	0	2872	1740	2682	1448
<u>Plume diameter[†] 120 yrs</u> (km)	3266	-	4559	2872	2782	-	3392	3266	3198	-	-	-	-	3393	3571	-

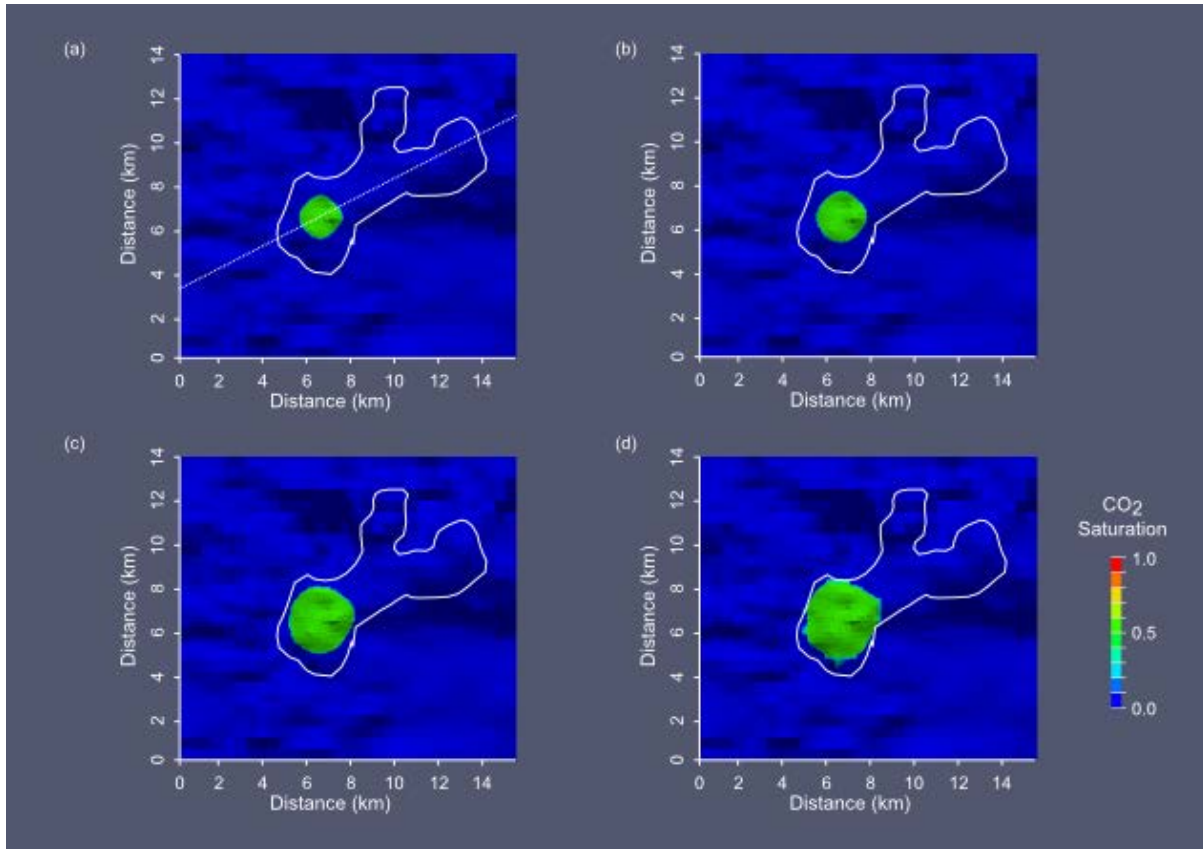
368

369

370

371 **Table 2.** Summary of model configurations and results. *Pressure measured at top of reservoir along
372 cross section line. †Plume diameter measured at top of reservoir along cross section line

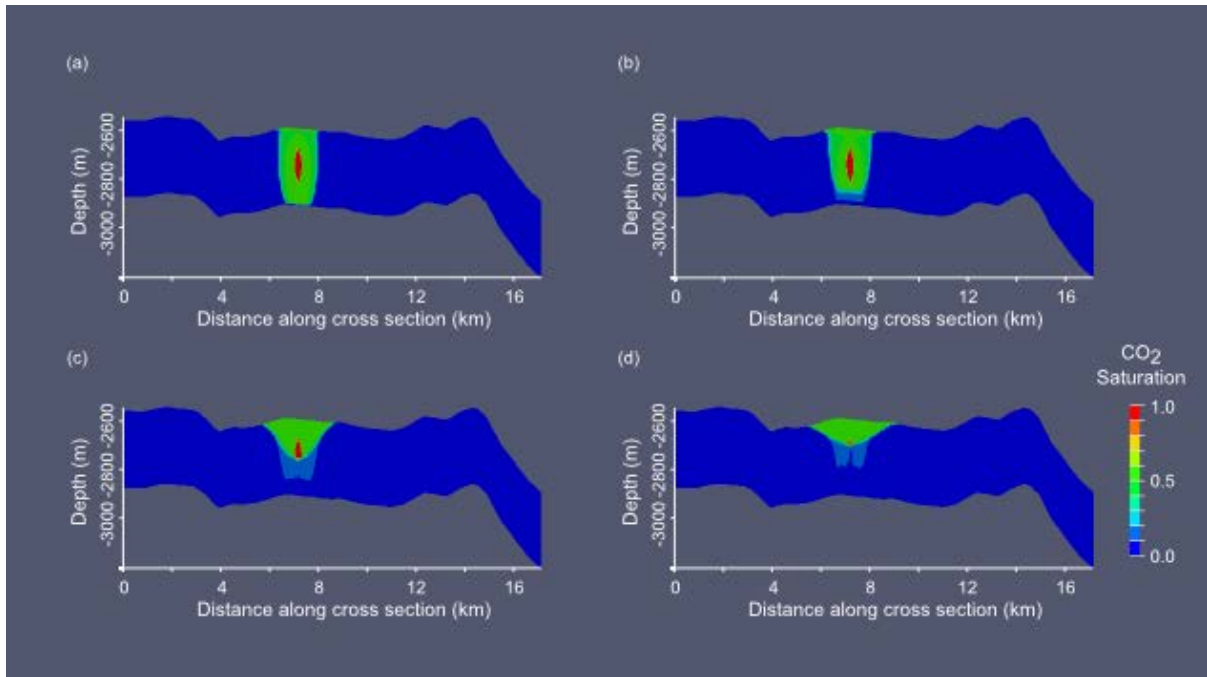
373 Table 2 shows the configuration of all models run and a summary of the results.



374

375 **Fig. 3.** s01a – CO₂ saturation at the top of the storage site, (a) 20 years, (b) 30 years, (c) 70 years, (d)
376 120 years. Shading indicates surface topography. White line indicates outline of CCC Prospect. White
377 dashed line indicates location of cross-section in Figs. 4, 11, 12, 13.

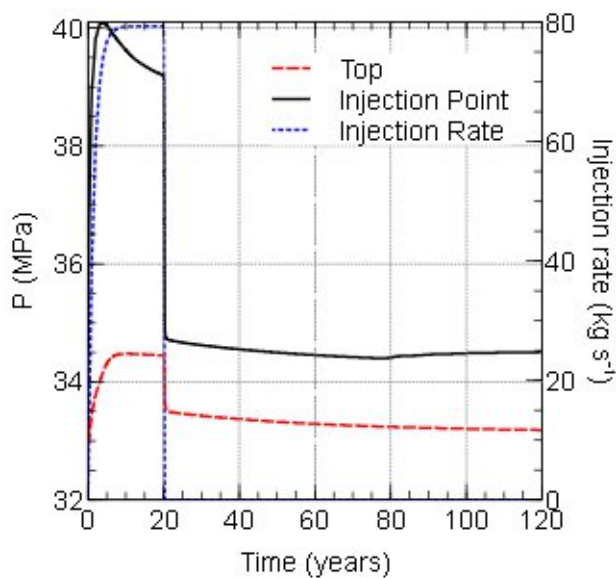
378 Fig. 3 shows the extent of the CO₂ plume, beneath the top of the storage site, through time for the
379 base case scenario (See Table 2, (s01a) - 320 m thick, open lateral and base boundaries, most likely
380 porosity and permeability values). The white line indicates the outline of the CCC Prospect at spill
381 point taken from the depth converted seismic. All the CO₂ is contained within the structure up to
382 100 years after the end of injection. However, the CO₂ plume is close to the edge of the structure at
383 the end of the simulation and in time may migrate out of it.



384

385 **Fig. 4.** *s01a* - CO₂ saturation for a cross section through the storage site, (a) 20 years, (b) 30 years, (c)
 386 70 years, (d) 120 years. 10 x vertical exaggeration. Cross section location shown in Fig. 3.

387 A cross section through the plume (Fig. 4) shows that CO₂ concentration is highest around the
 388 injection point. At the end of 20 years of injection CO₂ fills the whole thickness of the storage site.
 389 After injection finishes the plume migrates upwards under buoyancy and spreads laterally beneath
 390 the caprock. The CO₂ does not appear to have stabilised by this time, which would be indicated by
 391 the base of the CO₂ saturated part of the reservoir being level. It is most likely that the CO₂ will
 392 migrate into the dip closure to the right of the injection point (at ~ 14 km along the cross section)
 393 following the path with the highest stratigraphic relief.

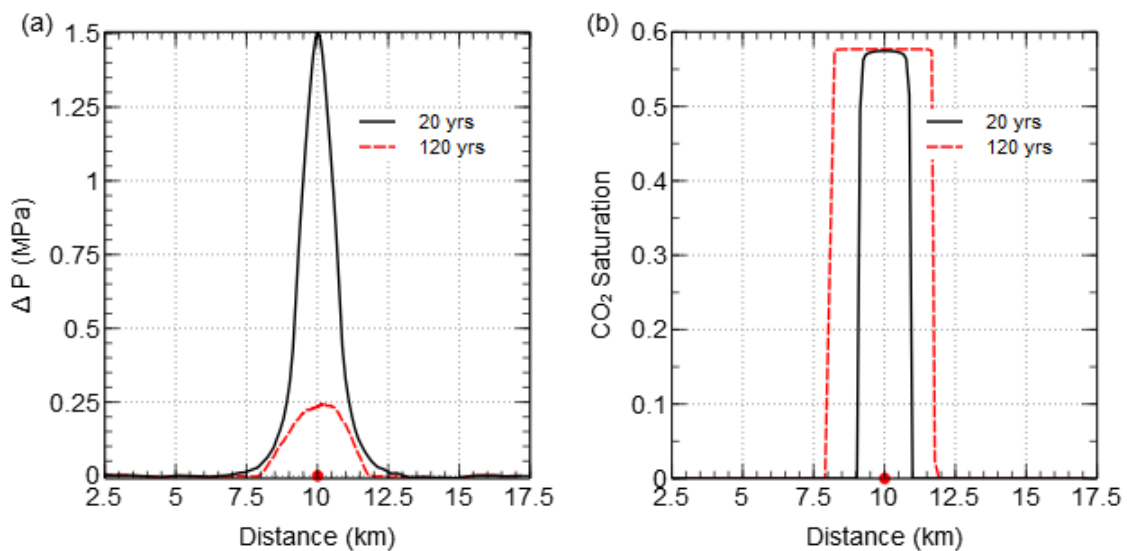


394

395 **Fig. 5.** *s01a* (see Table 2)- Pressure (P) through time for location immediately to the east of the
 396 injection point and at the top of the storage site above the injection point. Injection rate is also
 397 shown.

398 Fig. 5 shows the pressure through time next to the injection point and at the top of the storage site,
 399 directly above the injection point. Injection rate is also shown. At both locations the pressure
 400 increases as the cumulative amount of injected CO_2 increases. Near the injection point pressure
 401 peaks at 40.1 MPa after 4 years and then decreases. At the top of the storage site pressure increases
 402 more slowly and reaches a peak of 35.5 MPa at around 10 years. Pressure in all locations never
 403 exceeds the caprock fracture pressure of 47 MPa.

404 The initial pressure peak during the injection period is probably related to modelling effects
 405 associated with a rapid increase in pressure when the injection begins (see Mathias *et al.* 2011). It
 406 can be reduced by further shaping of the injection rate or a reduction in grid resolution around the
 407 injection point. Detailed modelling of injection has not been attempted in this study therefore
 408 maximum pressures for subsequent models have been taken at the end of the injection period
 409 where this effect is reduced.



410
 411 **Fig. 6.** *s01a* (see Table 2) - (a) Pressure buildup (ΔP) and (b) CO_2 saturation, along cross section at
 412 the top of the storage site. Injection point indicated by the red circle. Cross section location shown in
 413 Fig. 3.

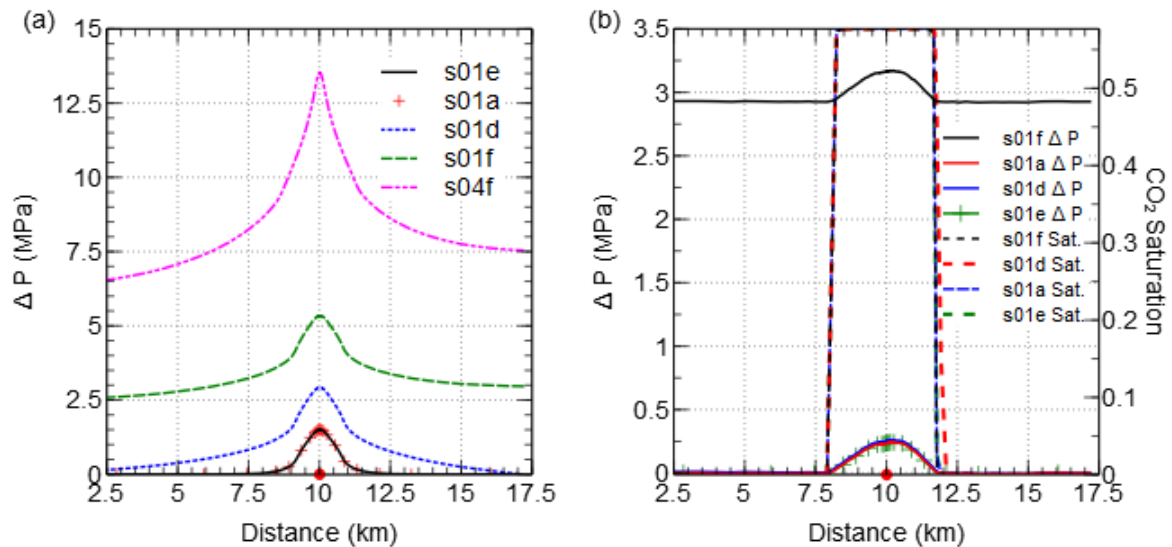
414 The pressure increase at the top of the storage site, along the line of the cross section, can be seen
 415 in Fig. 6(a). At the end of injection (20 years) the highest pressure increase is 1.50 MPa above virgin
 416 pressure, located above the injection point. Fig. 6(b) shows the extent of the CO_2 plume at the top of
 417 the storage site. It can be seen that the pressure increase extends approximately 3 km on either side
 418 of the CO_2 plume. In the rest of the model pressure has returned to its starting value. After 120
 419 years the pressure increase is 0.28 MPa. The highest pressure increase corresponds to the location
 420 of a structural stratigraphic high in the model where the CO_2 column beneath the caprock is thickest.

421 The pressure increase does not extend further than the edge of the CO₂ plume at the end of the
422 simulation.

423 Sensitivities

424 *Boundary conditions*

425 As the boundary conditions of the sides and the base of the model are not well constrained, several
426 models have been run to test the sensitivity of results to a change in boundary conditions.



427

428 **Fig. 7. (a)** Pressure buildup (ΔP) along cross section at the top of the storage site for models with
429 different boundary conditions at 20 years. Injection point indicated by the red circle. (b) Pressure
430 buildup and CO₂ saturation (Sat.) along cross section at the top of the storage site, for models with
431 different boundary conditions, at 120 years. s01a – open base, open sides, s01d – closed base, open
432 sides, s01e – open base, closed sides, s01f – closed base, closed sides, s04f – closed base, closed sides,
433 thin storage site (see Table 2). Injection point indicated by the red circle. Cross section location shown
434 in Fig. 3.

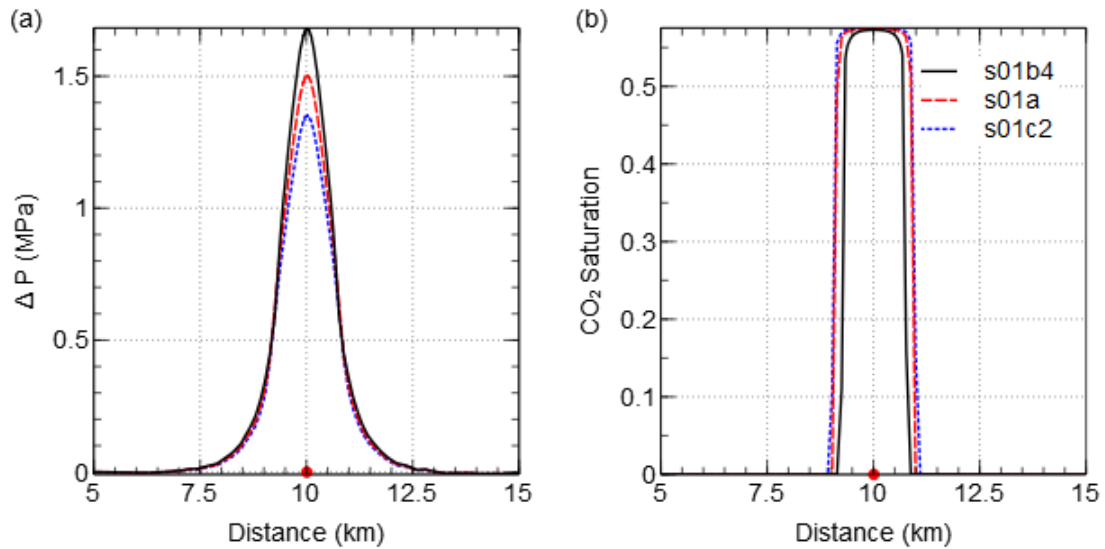
435 The pressure buildup at the end of injection is smallest for models with open (constant pressure)
436 base boundaries (Fig. 7(a)). For the two models run with open base boundaries the pressure increase
437 is almost identical at 20 years, regardless of the nature of the lateral boundaries. Having closed
438 boundaries on all sides of the model leads to a higher pressure buildup with a maximum pressure
439 increase of 5.34 MPa above the injection point.

440 The thickness of the storage site is unknown. Therefore a worst case scenario model was developed
441 with a relatively thin storage site (120 m) and closed boundaries on all sides. Pressure buildup in this
442 model is much higher than in other models (Fig. 7(a)). The pressure reaches a value of 46.5 MPa at
443 the end of injection, which is very close to the estimated caprock fracture pressure of 47 MPa. The
444 peak in pressure is located above the injection point.

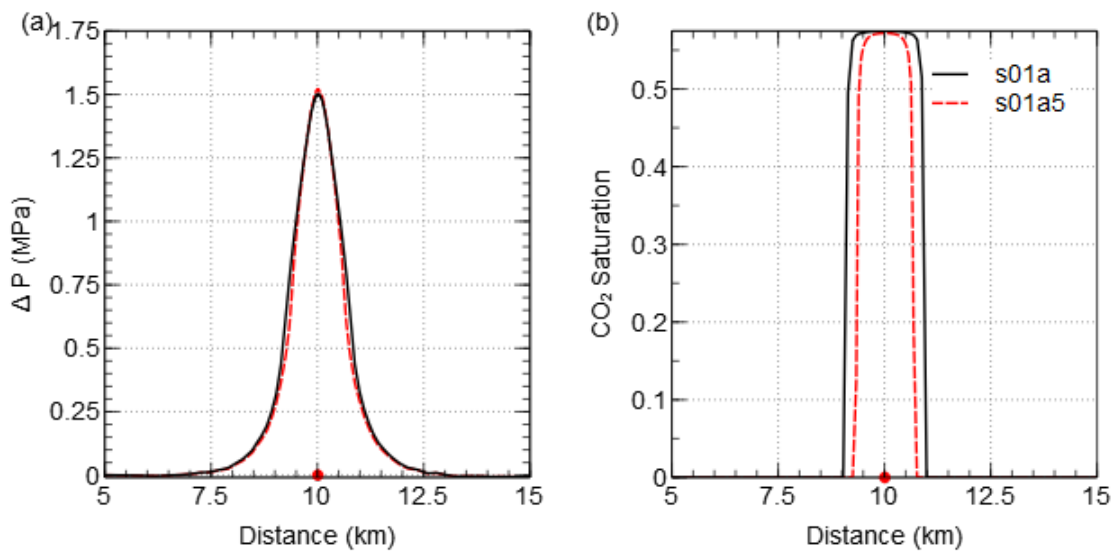
445 After 120 years the pressure has returned to starting pressure everywhere except beneath the CO₂
446 plume, for models with at least one open boundary (Fig. 7(b)). The pressure profile is the same for all

447 models but pressures in the model with closed side and base boundaries are approximately 2.9 MPa
 448 higher than pressures in the other models. The plume diameter at 120 years is very similar in all
 449 models.

450 **Permeability / Porosity**
 451



452
 453 **Fig. 8. (a)** Pressure buildup (ΔP) and **(b)** CO₂ saturation, along cross section at the top of the storage
 454 site, for models with different permeability, at 20 years. s01a – Most likely permeability, s01b4 –
 455 Min. permeability, s01c2 – Max. permeability (see Table 2). Injection point indicated by the red circle.
 456 Cross section location shown in Fig. 3.

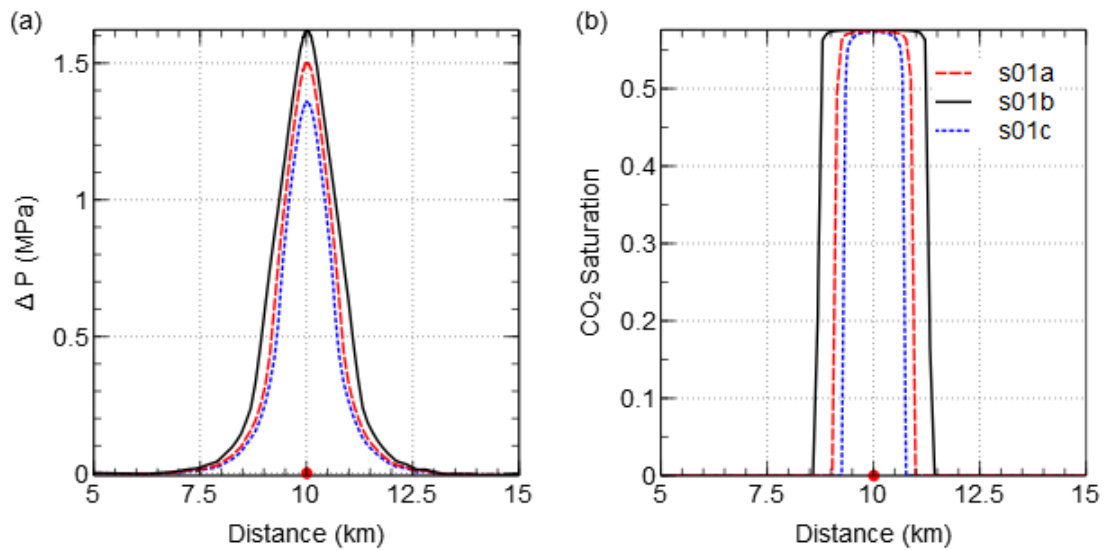


457

458 **Fig. 9. (a)** Pressure buildup (ΔP) and **(b)** CO₂ saturation, along cross section at the top of the storage
 459 site, for models with different porosity, at 20 years. s01a – Most likely porosity, s01a5 – Max.
 460 porosity. Location of injection point indicated by the red circle. Cross section location shown in Fig. 3.

461

462 Models were run with minimum and maximum permeability and porosity values in addition to the
 463 most likely values used in the base case. Lowering the permeability results in an increase in pressure
 464 buildup and a decrease in plume diameters after 20 years (Fig. 8). Increasing porosity values leads to
 465 a small increase in maximum pressure buildup. Having a higher porosity reduces the plume diameter
 466 at the top of the model after 20 years (Fig. 9).



467

468 **Fig. 10. (a)** Pressure buildup (ΔP) and **(b)** CO₂ saturation, along cross section at the top of the
 469 storage site, for models with varying porosity and permeability, at 20 years. s01a – Most likely
 470 porosity / permeability, s01b4 – Min. porosity / permeability, s01c2 – Max. porosity / permeability
 471 (see Table 2). Location of injection point indicated by the red circle. Cross section location shown in
 472 Fig. 3.

473

474 The pressure buildup and plume diameters which occur when both the porosity and permeability
 475 are changed at the same time show an increase in pressure buildup and plume diameter when the
 476 permeability and porosity are lower (Fig. 10).

477 **Layering**

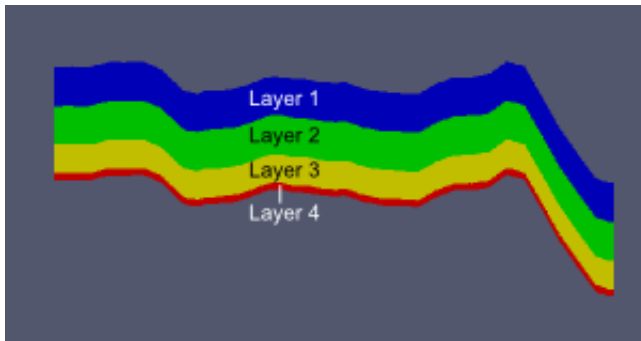
478

Facies	Thickness of layer (%)	Porosity (%)			Permeability (mD)		
		Min	Max	Mean	Min	Max	Mean
1. Fluvial	35	9	19	14	1	100	50.5
2. Aeolian	35	12	25	22	80	1000	540

3. Interdune	25	5	19	15	0.8	10	5.4
4. D facies	5	2	10	6	0.1	1	0.55

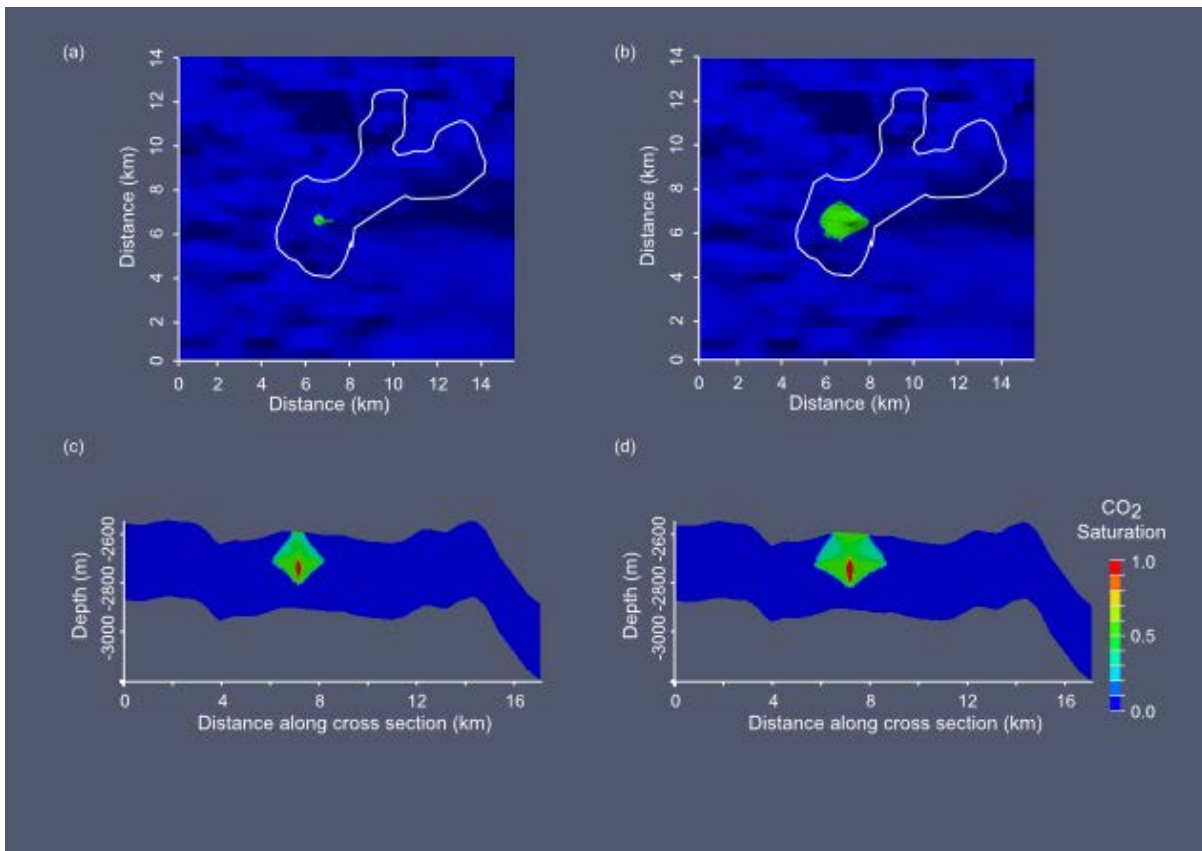
479 **Table 3.** Layer thicknesses and properties

480 Internal facies variation has been observed in Rotliegend reservoirs in the Auk and Argyll fields
 481 (Heward 1991; Heward *et al.* 2003). These variations have distinct permeability and porosity values
 482 which will affect fluid flow in the reservoir. A general layering scheme consisting of four layers has
 483 been derived from these papers, to represent possible layering in the Rotliegend at the location
 484 under investigation (Table 3). The thicknesses of layers have been defined as percentages to account
 485 for uncertainties in the total Rotliegend thickness.



486

487 **Fig. 11.** Slice through model showing layering. Numbers correspond to layers in Table 3. Red circle
 488 indicates location of injection point. 10 x vertical exaggeration. Cross section location shown in Fig. 1.



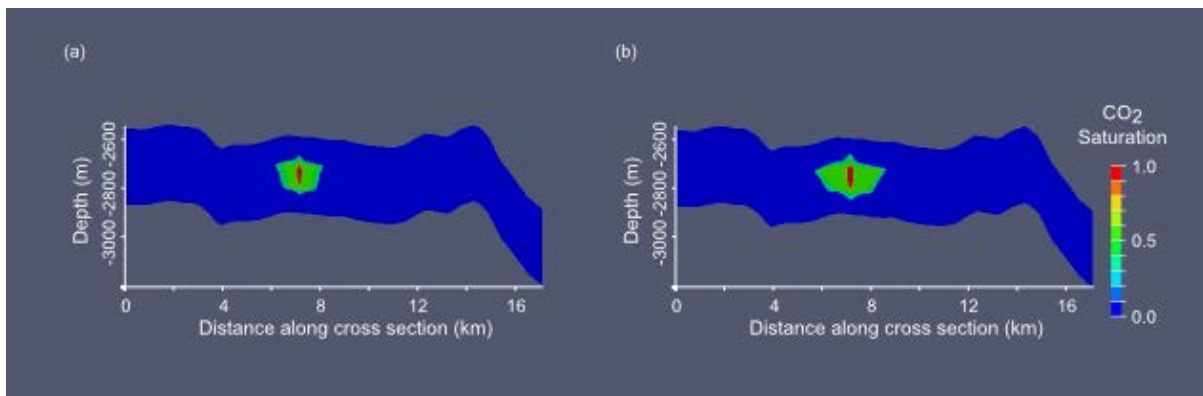
489

490 **Fig. 12** s02a2 – CO₂ saturation at the top of the storage site, for the layered storage site model, (a)
 491 10 years, (b) 20 yrs. White dots indicate outline of CCC prospect. CO₂ saturation for a cross section

492 through the layered storage site model (c) 10 years, (d) 20 yrs. 10 x vertical exaggeration. Cross
493 section location shown in Fig. 3.

494

495 Fig. 11 shows a cross section of the layered model. The presence of layers in the model modifies the
496 shape of the CO₂ plume as it rises towards the top of the storage site. The CO₂ spreads laterally
497 beneath the boundary between layers 1 and 2 (Fig. 12 (c) & (d)). This reduces the amount of CO₂
498 reaching the top of the storage site compared to the homogeneous model and therefore reduces
499 the plume diameter at the top of the model (Fig. 12 (a) & (b)). It can also be seen in Fig. 12 that the
500 CO₂ plume footprint is more irregular in shape than in other models. The plume spreads further to
501 the east of the injection point, following an area of high relief.



502

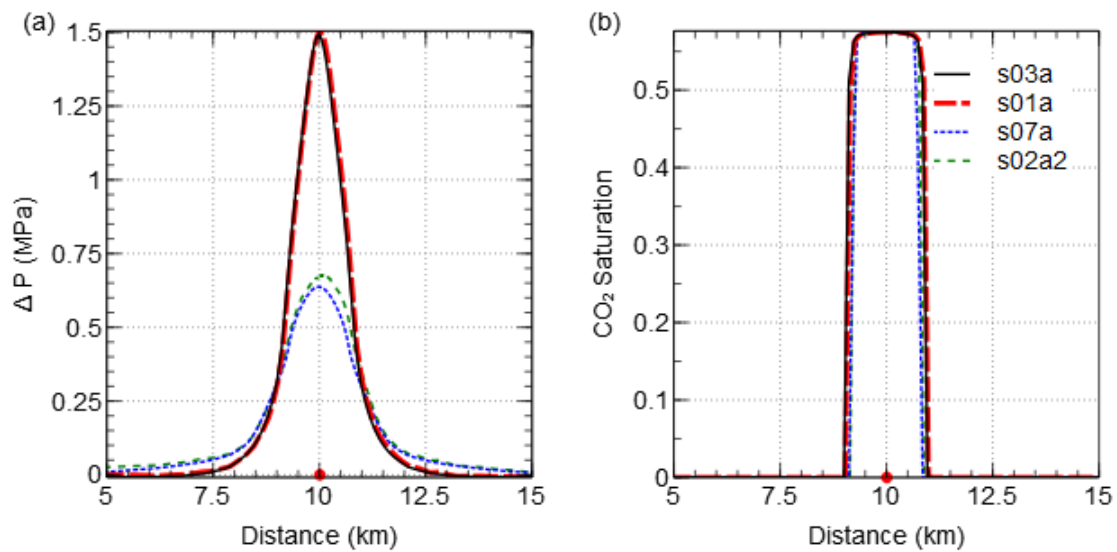
503 **Fig. 13.** s02a3 - CO₂ saturation for a cross section through the layered storage site model, with low
504 permeability, (a) 10 years and (b) 20 yrs. 10 x vertical exaggeration. Cross section location shown in
505 Fig. 3.

506

507 Permeability in the layered model has a large effect on the plume footprint and the pressure
508 buildup. When the permeability is higher the plume footprint is much larger than in the model with
509 average permeability. In the low permeability model the CO₂ does not reach the top of the model
510 after 20 years of injection. Nearly all the CO₂ is still contained within layer 2 (Fig. 13). The layers
511 reduce pressure buildup because they compartmentalise free CO₂; the exception being in the case
512 of the low permeability layered model, where the maximum pressure increase after 20 years
513 injection is nearly 2 MPa.

514 **Stratigraphic relief**

515 To assess the impact of irregular stratigraphic relief on results, two additional models were built with
516 flat, uniform surfaces, one with layers and one without.



517

518 **Fig. 14.** (a) Pressure buildup (ΔP) and (b) CO_2 saturation, along cross section at the top of the
 519 storage site, for flat and layered models, at 20 years. s03a – Flat, no layers, s01a – Irregular
 520 topography, no layers, s07a – Flat, layers, s02a2 – Irregular topography, layers (see Table 2).
 521 Location of injection point indicated by the red circle. Cross section location shown in Fig. 3.

522

523 Comparison of the non-layered models, both with and without irregular surfaces, shows that the
 524 effect of irregular stratigraphy on pressure buildup and plume spread is small (Fig. 14).

525 By contrast, in the layered models irregular stratigraphy has a noticeable effect on the pressure
 526 buildup and plume spread. In the flat, layered model the plume footprint and corresponding
 527 pressure buildup is symmetrical around the injection point. In the layered model with irregular
 528 stratigraphy the higher pressure buildup is observed in the region to the east of the injection point
 529 related to the irregular plume footprint shown in Fig. 12.

530 **Discussion**

531 **Pressure Buildup and Plume Diameter**

532 The largest pressure increases are observed in the models with closed boundaries on all sides. This is
 533 because the pressure buildup in the storage site is unable to dissipate (see Mathias *et al.* 2011).
 534 However, only in the thin, closed boundary model (s04f) is the pressure close to fracture pressure.
 535 Similar results have been found in other studies such as Hovorka *et al.* (2004) where the models with
 536 closed boundaries experienced the greatest pressure buildup. This situation, of a storage site with
 537 closed boundaries on all sides, is likely to be unrealistic for storage in a saline aquifer. Further data
 538 collection from the site should investigate how thick the storage site is, as well as ascertaining the
 539 nature of the base boundary of the storage site as these two factors appear to have the greatest
 540 influence on pressure buildup at this site.

541 The thickness of the Rotliegend at the CCC prospect could be better estimated if a well were drilled
 542 which completely penetrated the Rotliegend in the vicinity of the CCC prospect and reached the unit

543 beneath. The collection of 3D seismic data which could be tied to this well would allow a much
544 better estimate of the reservoir geometry. Hence, confidence in estimates of pressure buildup and
545 plume migration modelled using this data would be increased.

546 Increasing the permeability of the storage formation independently of porosity of the storage
547 formation reduces the pressure buildup seen at the top of the model (s01a, s01b4, s01c2). This
548 finding is similar to the results of Chadwick *et al.* (2009a) who showed that near-field pressure
549 (within a 2.5 m radius of the injection well) is inversely proportional to permeability. Increasing
550 storage formation porosity independently of permeability leads to slightly higher pressure at the top
551 of the model (s01a, s01a5). When both porosity and permeability are varied together, the models
552 with higher porosity and permeability exhibit lower pressure buildup (s01a, s01b, s01c).

553 Reducing the porosity of the storage site substantially increases the plume diameter at the top of
554 the storage site, with the largest plume diameter observed for the model with the lowest porosity.
555 This is because the same amount of CO₂ has to spread out further in a low porosity formation in
556 order to find enough pore space to be accommodated. Increasing the permeability of the storage
557 site without changing the porosity results in the plume diameter increasing. This result is supported
558 by the findings of Han *et al.* (2010) who showed that a larger area of the storage site is swept by CO₂
559 when the formation permeability is increased. Similarly Jahangiri & Zhang (2011) found that the
560 overall plume spread in all directions is increased when formation permeability is higher. Han *et al.*
561 (2010) also showed an increase in movement of CO₂ through the reservoir for lower permeability
562 ratio (k_v / k_h) which is likely to be the case for this reservoir although the permeability ratio has been
563 kept constant in our simulations.

564 Decreasing porosity and permeability together results in a larger plume diameter in our models at
565 the end of the simulation. For sandstones there is generally a strong positive correlation between
566 porosity and permeability and therefore porosity and permeability should be varied together. The
567 minimum permeability used in our models is higher than the permeability you would expect for a
568 reservoir with the corresponding minimum porosity (Glennie 1998). If the permeability was lower it
569 is likely that the plume diameter would be decreased and the pressure buildup increased. It will be
570 necessary then to have a better constraint on the relationship between porosity and permeability in
571 the reservoir in order to better predict the plume diameter.

572 The porosity and permeability values used in the most likely case are much closer to the values of
573 porosity and corresponding permeability that you would expect for Rotliegend Sandstone. The
574 plume diameter for the most likely case is within the CCC Prospect at the end of 120 years. However,
575 it is close to the edge of the CCC prospect and would probably migrate past the spill point after 120
576 years. The two main ways to stop this happening would be to fill the CCC prospect more effectively
577 and to increase dissolution and residual trapping within the reservoir. The CCC prospect could be
578 more effectively filled if the CO₂ were injected using multiple wells or a horizontal well which could
579 spread the CO₂ out over the whole area of the trap.

580 Ideally the porosity and permeability relationship in the reservoir could be investigated by collecting
581 and analysing well logs and core data at the site. Correlation of similar facies across multiple
582 locations throughout the site would allow a much more thorough understanding of the spatial
583 distribution of differing porosities and permeabilities. Subsequent modelling using the data would
584 provide a more detailed estimate of potential CO₂ migration. However, the nature of dynamic

585 modelling is such that if very detailed data were known it would still have to be upscaled somehow
586 and used to populate grid cells of approximately 10 m x 10 m. In consequence of this, whilst as much
587 porosity and permeability data as possible would be very useful, data on larger scales such as seismic
588 data, with one or two well ties, where porosity and permeability through the reservoir can be
589 deduced, would be more immediately applicable to building a dynamic model. Additionally, aside
590 from any issues relating to cost, it would be undesirable to have lots of wells drilled and core taken
591 from the site as this would increase the number of leakage pathways for CO₂ to escape to the
592 surface.

593 Dissolution and residual trapping have not been modelled in this study but they would reduce the
594 amount of free CO₂ within the plume and would therefore prevent the plume from spreading out so
595 far (Gasda *et al.* 2011). Some people have proposed ways of engineering the injection method to
596 increase these types of trapping. For example Qi *et al.* (2009) who suggested that injecting CO₂ with
597 brine and then injecting brine alone could increase residual trapping. The result of this would then
598 be an increase in dissolution trapping as the residually trapped CO₂ would dissolve in the brine
599 surrounding it.

600 Further modelling of the entire site up to and including the stratigraphic trap, would be useful to
601 determine the amount of CO₂ reaching the stratigraphic trap, and the time it would take to get there
602 if it leaks out of the CCC Prospect.

603 Looking at the effect of internal stratigraphic layering shows that pressure buildup at the top of the
604 model is reduced in the layered models. This is due to some CO₂ moving laterally beneath the
605 boundary between layers 1 and 2 away from the injection point. The resulting maximum pressure
606 buildup is reduced, as the CO₂ column above the injection point is thinned (Fig. 14). However, the
607 pressure increase affects a larger section of the reservoir because of the increased spread of CO₂
608 (Fig. 12). Core data from the site would give a much clearer indication of the layering present
609 beneath the CCC Prospect. Subsequent modelling using this information would provide a better
610 estimation of CO₂ migration at the site.

611 The effect of having a model with planar stratigraphy versus a model with irregular stratigraphy is
612 only apparent when comparing the layered models (s02a2, s07a). Here the influence of increased
613 stratigraphic relief leads to a more irregular plume shape with the plume extending further to the
614 east than in the flat layered model (Fig. 12(b)). A corresponding asymmetrical pressure profile can be
615 seen at the top of the model (Fig. 14(a)).

616 The irregular plume shape can be attributed to the movement of the CO₂ plume through the
617 reservoir from the injection point to the top of the storage site. After 10 years of injection, a small
618 amount of CO₂ has reached the top of the storage site above the injection point but some CO₂ has
619 spread along the layer boundary and pooled at an area of high stratigraphic relief, before rising to
620 the surface. The plume at top of the storage site has subsequently developed in an area slightly to
621 the east of the injection point, where there is a rise in the reservoir-caprock boundary, creating a
622 more irregular plume. Irregular plume shape, related to spreading of CO₂ along internal layering, has
623 been observed in modelling studies by Ghomian *et al.* (2008). It has also been inferred from seismic
624 data at Sleipner, where it can be seen that injected CO₂ is spreading beneath intraformational shale
625 layers, following areas of high relief of the stratigraphic boundaries (Arts *et al.* 2004).

626 In the homogeneous models and the flat layered model this has not happened as there is either no
627 internal layering, or the layering is regular and contains no areas of high relief. This means that the
628 CO₂ plume is still fairly regular in shape when it reaches the top of the storage site, leading to a
629 correspondingly regular plume footprint.

630 **Storage capacity**

631 The simulations indicate that the site is likely to have a large enough storage capacity to
632 accommodate injection of CO₂ at a rate of 2.5 Mt a⁻¹ for 20 years. This leads to a total storage
633 capacity of at least 50 Mt within the CCC Prospect. To put this into perspective, as of 2011, 12.7 Mt
634 of CO₂ had been stored in the North Sea at Sleipner over 15 years (Statoil 2011). 50 Mt is between
635 0.01 and 0.025 % of the total amount of CO₂ required to be stored by the UK before 2050.

636 Pressure buildup in the case of the thin storage site with the closed boundary is very close to
637 fracture pressure. If the storage site is thin with a closed boundary, it may be possible to prevent
638 pressures reaching such high values by engineering the injection scheme in some way. For instance
639 by injecting at a lower rate from multiple wells or by using a horizontal well which allows the CO₂ to
640 be spread more evenly throughout the CCC Prospect. A large proportion of the CCC Prospect, to the
641 north east, has not been filled. Further modelling should look at different injection schemes to
642 determine the best way of filling the structure to maximise storage capacity and minimise pressure
643 buildup.

644 **Comparison of results with static capacity estimates**

645 Hedley et al. (2013) used Monte-Carlo simulations to estimate static capacity at the site. Simulations
646 were run for differing values of porosity, gross rock volume (volume of the CCC prospect), residual
647 water saturation, maximum allowable pressure increase and efficiency factor. The efficiency factor is
648 a factor related to the proportion of the reservoir which is likely to be swept by invading CO₂.

649 For each set of simulated variables the theoretical, open and closed capacities were estimated. The
650 theoretical storage capacity is the pore volume of the reservoir, minus the residual water saturation,
651 multiplied by density of CO₂ at the appropriate pressure and temperature conditions. The open
652 storage capacity is the theoretical storage capacity multiplied by the efficiency factor. The closed
653 storage capacity is the additional pore volume created by compressing the existing brine and rock
654 within the reservoir up to the maximum allowable pressure buildup.

655 Statistics calculated from the results show that 80% of theoretical capacity estimates are in the
656 range 42 Mt – 112 Mt. For open storage capacity estimates the range of results reduces to 7.59 Mt
657 – 28 Mt. For closed storage capacity estimates 80% of the results were in the range 1.7 Mt – 3 Mt.

658 In comparison, dynamic modelling results indicate that for all models a storage capacity of 50 Mt can
659 be achieved without exceeding fracture pressure. Albeit coming very close to fracture pressure for
660 the closed thin system.

661 One reason for the large discrepancy between dynamic and static capacity estimates is that the
662 static estimates only involve the volume of the CCC prospect down to the depth of the spill point. In
663 the dynamic simulations there is CO₂ within the reservoir below the depth of the spill point. Once
664 this has migrated above the spill point it is possible that the CO₂ will flow laterally past the spill point
665 and leak from the CCC prospect, thereby reducing the modelled storage capacity. However, a large

666 volume of the CCC prospect to the north east has not been filled and it is more likely that CO₂ will
667 migrate up dip to the north east and fill the rest of the CCC prospect before moving down dip past
668 the spill point.

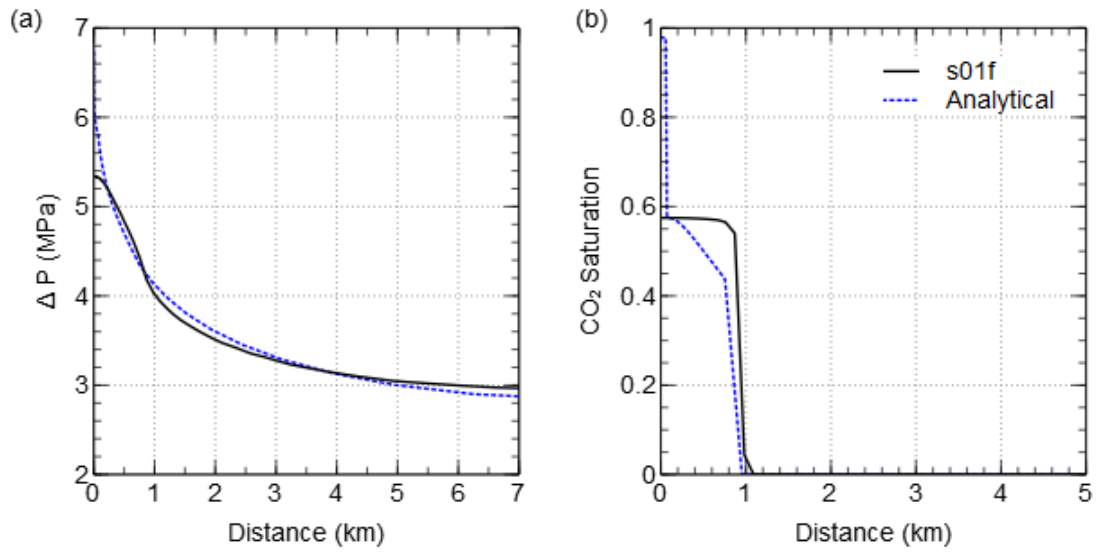
669 The presence of reservoir below the spill point will also have an effect on the capacity estimates for
670 a closed aquifer. For capacity estimates relating to closed aquifers the only available pore space
671 which can contain CO₂ is the additional pore space created by the compression of the brine and rock
672 within the CCC prospect. This essentially assumes an impermeable layer directly below the CCC
673 prospect at the level of the spill point. As the reservoir is likely to extend below the spill point the
674 compressibility of the brine and rock below the CCC prospect must also be taken into account,
675 increasing the extra pore space available to store CO₂.

676 Static capacity estimates for an open aquifer include a factor related to the sweep efficiency of the
677 aquifer. Sweep efficiency can be reduced by small scale permeability variations within the reservoir
678 which lead to preferential flow of CO₂ through areas with higher permeability. Sweep efficiency can
679 also be reduced by larger scale permeability variations in the reservoir related to the net to gross
680 ratio of the reservoir rocks. Additionally, sweep efficiency can be related to the geometry of the
681 stratigraphic layers and the tendency of the buoyant CO₂ to flow updip when it reaches a layer of
682 lower permeability. This may cause channelling of the CO₂ along areas of high relief (e.g. Arts *et al.*
683 2004).

684 The dynamic simulations do not include small scale permeability variations due to heterogeneities in
685 the sandstones or values of net to gross. Therefore they are likely to overestimate sweep efficiency in
686 the reservoir.

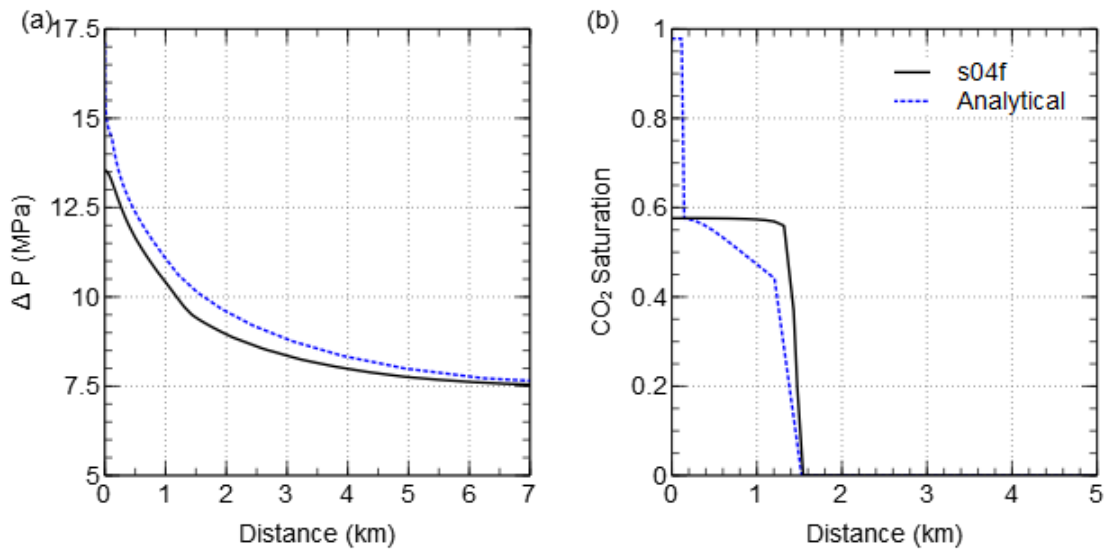
687 Static capacity estimates provide a way to quickly model many variations in reservoir parameters.
688 However, there is a large discrepancy between the storage capacities predicted by the static models
689 and those predicted by the dynamic models. This is primarily due to the fairly restrictive assumptions
690 involved in the static capacity estimates. For instance the assumption of brine compressibility only
691 within the trap in the case of a closed system is likely to be unrealistic in this case as we know the
692 reservoir extends below the CCC prospect. Additionally the sweep efficiency factors used to estimate
693 the open capacity of the trap are difficult to quantify without carrying out some form of dynamic
694 modelling as well.

695 **Comparison of results with analytical solutions for plume diameter and pressure buildup**
696 Mathias et al. (2011) derived an analytical solution for calculating plume diameter and pressure
697 buildup assuming vertical equilibrium. The analytical solution assumes that the side and base
698 boundaries of the reservoir are impermeable.



699

700 **Fig. 15** Comparison of results of dynamic modelling from this study with the analytical solution of
 701 Mathias et al. (2011). Reservoir is 320 m thick, injection well is at 0km **(a)** Change in pressure. **(b)** CO₂
 702 saturation.



703

704 **Fig. 16** Comparison of results of dynamic modelling from this study with the analytical solution of
 705 Mathias et al. (2011). Reservoir is 120 m thick, injection well is at 0km **(a)** Change in pressure. **(b)** CO₂
 706 saturation.

707

708 Figs. 15 & 16 show the comparison of the analytical solution with the corresponding dynamic
 709 solution for a reservoir thickness of 320 m and 120 m respectively. For both cases the pressure
 710 buildup predicted by the analytical model is slightly higher directly above the injection point. The
 711 plume diameters predicted by both models are very similar in both cases. The analytical model also

712 predicts a value for CO₂ saturation around the injection point which is higher than one minus the
713 residual water saturation. This is due to the analytical solution modelling the dryout front, behind
714 which the residual water has all dissolved into the CO₂ stream. The dynamic models also display this
715 behaviour around the injection point but not at the surface where the results in Figs. 15 & 16 are
716 taken from.

717 It can be seen that the analytical solutions provide very similar results to the dynamic models in
718 certain situations. However, the main limitation is the fact that the analytical solutions can only be
719 used to model certain situations i.e. where the storage site is surrounded by impermeable
720 boundaries and where there is no internal heterogeneity.

721 **Choice of dynamic modelling method**

722 Using a full 3D numerical model has allowed us to produce results for storage capacity, pressure
723 buildup and plume migration which include both the effects of vertical heterogeneity within the
724 storage site and the geometry of the storage site. Using other dynamic modelling methods (e.g.
725 streamline, vertical equilibrium etc.) would also give us indications of storage capacity, pressure
726 buildup and plume migration. However, the large pressure change due to injection was considered
727 unsuitable to be dealt with using streamline simulations. Additionally, the need to account for
728 vertical layering and permeability anisotropy rendered vertical equilibrium modelling inappropriate.
729 We have found that the combined presence of internal stratigraphic layering and stratigraphic relief
730 has a noticeable impact on plume migration. Although we are not able to confidently predict plume
731 migration at this stage, due to uncertainties in the input data, our modelling work indicates that the
732 presence and properties of any stratigraphic layers in the storage site and the relief of potential
733 layers are major influences on plume migration at the site. This supports the findings of several
734 other case studies (e.g. Arts *et al.* 2004; Hovorka *et al.* 2004; Zhou *et al.* 2010). Therefore when
735 entering the next stage of the project, more data should be collected regarding internal porosity and
736 permeability variations within the reservoir and the stratigraphic relief of the site to facilitate more
737 accurate modelling of CO₂ migration.

738 **Conclusions**

739 In this study we have created a preliminary dynamic model of a potential CO₂ storage site, within a
740 deep saline formation, of the Rotliegend sandstones of the UK North Sea. Model properties have
741 been derived from a limited set of primary data from the site, and from literature and well log data
742 from nearby locations.

743 Our modelling results indicate that the site can store ~2.5 Mt a⁻¹ of CO₂ over a period of 20 years
744 without injected CO₂ reaching the containment spill point or the pressure exceeding the caprock
745 fracture pressure, for up to 100 years after injection. A large section of the CCC structure has not
746 been filled

747 The main controls on pressure buildup are the nature of the base boundary of the storage reservoir
748 and the thickness of reservoir at the storage site. The main controls on plume diameter are the
749 porosity, permeability and permeability anisotropy ratio of the formation.

750 The major uncertainties at the site are the properties of the unit beneath the Rotliegend at the
751 location of the CCC Prospect and the thickness of the Rotliegend at the CCC Prospect. Further data

752 collection, such as the acquisition of a 3D seismic data set, tied to well data within the storage site,
753 would assist in improving our understanding of these two parameters.

754 A thorough understanding of the porosity and permeability structure within the storage site would
755 allow a much better estimate of plume migration pathways and plume diameter. To facilitate this
756 more well and core data should be collected in the vicinity of the storage site. A compromise needs
757 to be made between maximising the number of wells which can be drilled at the site and minimising
758 the man-made leakage pathways for CO₂. Furthermore, it should be noted that for the purpose of
759 dynamic modelling, data regarding small scale porosity and permeability variations (i.e. < 10 m
760 resolution) will have to be scaled up and aggregated using a methodology similar to that described in
761 this work, in order to populate a dynamic model. As a consequence, the acquisition of a high
762 resolution seismic dataset in conjunction with a small number of well and core datasets would be
763 more useful for building a dynamic model, than, for instance, collecting lots of core data without
764 finding out any more information regarding the geometry and boundaries of the storage site.

765 Overall, the site looks promising for CO₂ storage and warrants some further investigation. Modelling
766 using more detailed information will improve estimates for plume migration and pressure buildup.
767 These models can then be used to test ways of filling the structure more efficiently, for instance with
768 different injection locations, numbers of wells, and injection rates, in order to maximise CO₂ storage
769 capacity and minimise pressure buildup within the CCC Prospect.

770 A comparison between static and dynamic modelling of the site for CO₂ sequestration shows that
771 generally the dynamic capacity estimates exceed the static capacity estimates. This mainly due to
772 the assumptions required to calculate static capacity estimates which are not necessarily true and
773 are not required for the dynamic modelling. Analytical estimates of pressure buildup and plume
774 diameter are very quick to calculate and provide a close match with dynamic models for scenarios
775 with closed boundaries however they are not suitable for modelling other situations such as a
776 reservoir with open boundaries or internal heterogeneity.

777 3D, grid based, numerical modelling has been useful as it has allowed us to identify and prioritise
778 factors which could have a strong influence on the behaviour of CO₂ at the site even though only
779 limited site data is available. This information will dictate the planning of future site characterisation
780 work.

781 The authors would like to thank Progressive Energy Ltd. and TGS-NOPEC for access to seismic data.
782 The authors would also like thank David Noy for his assistance with TOUGH2.

783 **References**

784 Arts, R. 2004. Monitoring of CO₂ injected at Sleipner using time-lapse seismic data. *Energy*, **29**(9-10),
785 1383–1392, doi:10.1016/j.energy.2004.03.072

786 Bennion, D. B. & Bachu, S. 2006. Supercritical CO₂ and H₂S – Brine Drainage and Imbibition Relative
787 Permeability Relationships for Intergranular Sandstone and Carbonate Formations. *Society of*
788 *Petroleum Engineers Paper 99326*.

789 Bentham, M. 2006. An assessment of carbon sequestration potential in the UK – Southern North Sea
790 case study. *Tyndall Centre for Climate Change Research Working Paper 85*.

791 Boait, F. C., White, N. J., Bickle, M. J., Chadwick, R. A., Neufeld, J. A. & Huppert, H. E. 2012. Spatial
792 and temporal evolution of injected CO₂ at the Sleipner Field, North Sea. *Journal of Geophysical*
793 *Research*, **117**(B3), 1–21, doi:10.1029/2011JB008603

794 Chadwick, R. A., Noy, D. J. & Holloway, S. 2009a. Flow processes and pressure evolution in aquifers
795 during the injection of supercritical CO₂ as a greenhouse gas mitigation measure. *Petroleum*
796 *Geoscience*, **15**(1), 59–73, doi:10.1144/1354-079309-793

797 Chadwick, R. A., Noy, D., Arts, R. & Eiken, O. 2009b. Latest time-lapse seismic data from Sleipner
798 yield new insights into CO₂ plume development. *Energy Procedia*, **1**(1), 2103–2110,
799 doi:10.1016/j.egypro.2009.01.274

800 Chasset, C., Jarsjö, J., Erlström, M., Cvetkovic, V. & Destouni, G. 2011. Scenario simulations of CO₂
801 injection feasibility, plume migration and storage in a saline aquifer, Scania, Sweden. *International*
802 *Journal of Greenhouse Gas Control*, **5**(5), 1303–1318, doi:10.1016/j.ijggc.2011.06.003

803 Cornford, C. 1990. Source Rocks and Hydrocarbons of the North Sea. In K W Glennie (Ed.),
804 *Introduction to the Petroleum Geology of the North Sea* (Third., pp. 294–361). Blackwell Science Ltd.

805 DECC. 2012. CCS Roadmap. Department of Energy and Climate Change.

806 Doughty, C. 2007. Modeling geologic storage of carbon dioxide: Comparison of non-hysteretic and
807 hysteretic characteristic curves. *Energy Conversion and Management*, **48**(6), 1768–1781,
808 doi:10.1016/j.enconman.2007.01.022

809 Doughty, C. 2010. Investigation of CO₂ plume behavior for a large-scale pilot test of geologic carbon
810 storage in a saline formation. *Transport in Porous Media*, **82**(1), 49–76, doi:10.1007/s11242-009-
811 9396-z

812 Eigestad, G. T., Dahle, H. K., Hellevang, B., Riis, F., Johansen, W. T. & Øian, E. 2009. Geological
813 modeling and simulation of CO₂ injection in the Johansen formation. *Computational Geosciences*,
814 **13**(4), 435–450, doi:10.1007/s10596-009-9153-y

815 Gasda, S. E., Nordbotten, J. M. & Celia, M. A. 2009. Vertical equilibrium with sub-scale analytical
816 methods for geological CO₂ sequestration. *Computational Geosciences*, **13**(4), 469–481,
817 doi:10.1007/s10596-009-9138-x

818 Gasda, S. E., Nordbotten, J. M. & Celia, M. A. 2011. Vertically averaged approaches for CO₂ migration
819 with solubility trapping. *Water Resources Research*, **47**(5), 1–14, doi:10.1029/2010WR009075

820 Ghomian, Y., Pope, G. & Sepehrnoori, K. 2008. Reservoir simulation of CO₂ sequestration pilot in Frio
821 brine formation, USA Gulf Coast. *Energy*, **33**(7), 1055–1067, doi:10.1016/j.energy.2008.02.011

822 Glennie, K.W. 1983. Early Permian (Rotliegendes) palaeowinds of the north sea. *Sedimentary*
823 *Geology*, **34**(2-3), 245–265. doi:10.1016/0037-0738(83)90088-X

824 Glennie, K.W., Higham, J. & Stemmerik, L. 2003. Permian. In D. Evans, C. Graham, A. Armour, & P.
825 Bathurst (Eds.), *The Millennium Atlas: petroleum geology of the central and northern North Sea*. (pp.
826 91–103). London: Geological Society of London.

- 827 Han, W. S., Lee, S.-Y., Lu, C. & McPherson, B. J. 2010. Effects of permeability on CO₂ trapping
828 mechanisms and buoyancy-driven CO₂ migration in saline formations. *Water Resources Research*,
829 **46**(7), 1–20, doi:10.1029/2009WR007850
- 830 Hatzignatiou, D. G., Riis, F., Berenblyum, R., Hladik, V., Lojka, R. & Francu, J. 2011. Screening and
831 evaluation of a saline aquifer for CO₂ storage: Central Bohemian Basin, Czech Republic. *International*
832 *Journal of Greenhouse Gas Control*, **5**(6), 1429–1442, doi:10.1016/j.ijggc.2011.07.013
- 833 Heinemann, N., Wilkinson, M., Pickup, G. E., Haszeldine, R. S. & Cutler, N. a. 2012. CO₂ storage in the
834 offshore UK Bunter Sandstone Formation. *International Journal of Greenhouse Gas Control*, **6**, 210–
835 219, doi:10.1016/j.ijggc.2011.11.002
- 836 Heward, A. P. 1991. Inside Auk - The anatomy of an eolian oil reservoir. In A. D. Miall & N. Tyler
837 (Eds.), *The Three-Dimensional Facies Architecture of Terrigenous Clastic Sediments and Its*
838 *Implications for Hydrocarbon Discovery and Recovery* (pp. 44–56), doi:10.2110/csp.91.03.0044
- 839 Heward, A. P., Schofield, P. & Gluyas, J. G. 2003. The Rotliegend reservoir in Block 30/24, UK Central
840 North Sea: including the Argyll (renamed Ardmore) and Innes fields. *Petroleum Geoscience*, **9**(4),
841 295–307, doi:10.1144/1354-079303-578
- 842 Hovorka, S. D., Doughty, C., Benson, S. M., Pruess, K. & Knox, P. R. 2004. The impact of geological
843 heterogeneity on CO₂ storage in brine formations: a case study from the Texas Gulf Coast.
844 *Geological Society, London, Special Publications*, **233**(1), 147–163,
845 doi:10.1144/GSL.SP.2004.233.01.10
- 846 IPCC. 2005. Carbon Dioxide Capture and Storage. (B. Metz, O. Davidson, H. de Coninck, M. Loos, & L.
847 Meyer, Eds.). Cambridge University Press.
- 848 Jahangiri, H. R. & Zhang, D. 2011. Effect of spatial heterogeneity on plume distribution and dilution
849 during CO₂ sequestration. *International Journal of Greenhouse Gas Control*, **5**(2), 281–293,
850 doi:10.1016/j.ijggc.2010.10.003
- 851 Jalalh, A. A. 2006. Compressibility of porous rocks: Part II. New relationships. *Acta Geophysica*, **54**(4),
852 399–412, doi:10.2478/s11600-006-0029-4
- 853 Jin, M., Pickup, G., Mackay, E., Todd, A., Monaghan, A., Survey, B. G. & Naylor, M. 2010. Static and
854 Dynamic Estimates of CO₂ Storage Capacity in Two Saline Formations in the UK. *Society of Petroleum*
855 *Engineers Paper 131609*.
- 856 Mathias, S. A., Gluyas, J. G., Oldenburg, C. M. & Tsang, C.-F. 2010. Analytical solution for Joule–
857 Thomson cooling during CO₂ geo-sequestration in depleted oil and gas reservoirs. *International*
858 *Journal of Greenhouse Gas Control*, **4**(5), 806–810, doi:10.1016/j.ijggc.2010.05.008
- 859 Mathias, S. A., González Martínez de Miguel, G. J., Thatcher, K. E. & Zimmerman, R. W. 2011.
860 Pressure Buildup During CO₂ Injection into a Closed Brine Aquifer. *Transport in Porous Media*, **89**(3),
861 383–397, doi:10.1007/s11242-011-9776-z

862 Mathias, S. A., Hardisty, P. E., Trudell, M. R. & Zimmerman, R. W. 2008. Approximate Solutions for
863 Pressure Buildup During CO₂ Injection in Brine Aquifers. *Transport in Porous Media*, **79**(2), 265–284,
864 doi:10.1007/s11242-008-9316-7

865 Møll Nilsen, H., Herrera, P. A., Ashraf, M., Ligaarden, I., Iding, M., Hermanrud, C., Lie, K.-A., et al.
866 2011. Field-case simulation of CO₂ -plume migration using vertical-equilibrium models. *Energy*
867 *Procedia*, **4**, 3801–3808, doi:10.1016/j.egypro.2011.02.315

868 Narasimhan, T. N. & Witherspoon, P. A. 1976. An Integrated Finite Difference Method for Analyzing
869 Fluid Flow. *Water Resources Research*, **12**(1), 57–64.

870 Nordbotten, J. M., Celia, M. A. & Bachu, S. 2005. Injection and Storage of CO₂ in Deep Saline
871 Aquifers: Analytical Solution for CO₂ Plume Evolution During Injection. *Transport in Porous Media*,
872 **58**(3), 339–360, doi:10.1007/s11242-004-0670-9

873 Noy, D. J., Holloway, S., Chadwick, R. A., Williams, J. D. O., Hannis, S. A. & Lahann, R. W. 2012.
874 Modelling large-scale carbon dioxide injection into the Bunter Sandstone in the UK Southern North
875 Sea. *International Journal of Greenhouse Gas Control*, **9**, 220–233, doi:10.1016/j.ijggc.2012.03.011

876 Obi, E. I. & Blunt, M. J. 2006. Streamline-based simulation of carbon dioxide storage in a North Sea
877 aquifer. *Water Resources Research*, **42**(3), doi:10.1029/2004WR003347

878 Oldenburg, C. 2007. Joule-Thomson cooling due to CO₂ injection into natural gas reservoirs. *Energy*
879 *Conversion and Management*, **48**(6), 1808–1815, doi:10.1016/j.enconman.2007.01.010

880 Pacala, S. & Socolow, R. 2004. Stabilization wedges: solving the climate problem for the next 50
881 years with current technologies. *Science (New York, N.Y.)*, **305**(5686), 968–72,
882 doi:10.1126/science.1100103

883 Pruess, K. 2005. ECO2N: A TOUGH2 Fluid Property Module for Mixtures of Water, NaCl, and CO₂.
884 *Lawrence Berkeley National Laboratory Report LBNL-57952*.

885 Pruess, K., García, J., Kovscek, T., Oldenburg, C., Rutqvist, J., Steefel, C. & Xu, T. 2004. Code
886 intercomparison builds confidence in numerical simulation models for geologic disposal of CO₂.
887 *Energy*, **29**, 1431–1444, doi:10.1016/j.energy.2004.03.077

888 Pruess, K., Oldenburg, C. & Moridis, G. 1999. TOUGH2 User's Guide, Version 2.0. *Lawrence Berkeley*
889 *National Laboratory Report LBNL-43134*.

890 Qi, R., Laforce, T. & Blunt, M. 2009. Design of carbon dioxide storage in aquifers. *International*
891 *Journal of Greenhouse Gas Control*, **3**(2), 195–205, doi:10.1016/j.ijggc.2008.08.004

892 Ringrose, P., Nordahl, K., & Wen, R. 2005. Vertical permeability estimation in heterolithic tidal deltaic
893 sandstones. *Petroleum Geoscience*, **11**(1), 29–36.

894 Schäfer, F., Walter, L., Class, H. & Müller, C. 2012. The regional pressure impact of CO₂ storage: a
895 showcase study from the North German Basin. *Environmental Earth Sciences*, **65**(7), 2037–2049,
896 doi:10.1007/s12665-011-1184-8

- 897 Selley, R. C. 1978. Porosity gradients in North Sea oil-bearing sandstones. *Journal of the Geological*
898 *Society*, **135**(1), 119–132, doi:10.1144/gsjgs.135.1.0119
- 899 Spycher, N., & Pruess, K. 2005. CO₂–H₂O mixtures in the geological sequestration of CO₂. II.
900 Partitioning in chloride brines at 12–100 °C and up to 600 bar. *Geochimica et Cosmochimica Acta*, **69**,
901 3309–3320, doi:10.1016/j.gca.2005.01.015
- 902 Statoil. 2011. Statoil Annual Report. World Wide Web Address:
903 <http://www.statoil.com/AnnualReport2011>
- 904 Taylor, J. C. M. 1998. Upper Permian - Zechstein. In K. W. Glennie (Ed.), *Petroleum Geology of the*
905 *North Sea* (pp. 174 – 211). Oxford, UK: Blackwell Science Ltd., doi:10.1002/9781444313413
- 906 The European Union. 2009. Directive 2009/31/EC of the European Parliament and of the council.
907 *Official Journal of the European Union*.
- 908 Trewin, N. H., Fryberger, S. G. & Kreutz, H. 2003. The Auk Field, Block 30/16, UK North Sea. (J. G.
909 Gluyas & H. M. Hitchens, Eds.) *United Kingdom Oil and Gas Fields, Commemorative Millennium*
910 *Volume, Geological Society, London, Memoir*, **20**, 485–496.
- 911 Wyllie, M. R. J., Gregory, A. R., & Gardner, G. H. F. 1958. An experimental investigation of factors
912 affecting elastic wave velocities in porous media. *Geophysics*, **23**(3), 459–493.
- 913 Yamamoto, H. & Doughty, C. 2011. Investigation of gridding effects for numerical simulations of CO₂
914 geologic sequestration. *International Journal of Greenhouse Gas Control*,
915 doi:10.1016/j.ijggc.2011.02.007
- 916 Yamamoto, H., Zhang, K., Karasaki, K., Marui, A., Uehara, H. & Nishikawa, N. 2009. Numerical
917 investigation concerning the impact of CO₂ geologic storage on regional groundwater flow.
918 *International Journal of Greenhouse Gas Control*, **3**(5), 586–599, doi:10.1016/j.ijggc.2009.04.007
- 919 Yielding, G., Lykakis, N. & Underhill, J. R. 2011. The role of stratigraphic juxtaposition for seal
920 integrity in proven CO₂ fault-bound traps of the Southern North Sea. *Petroleum Geoscience*, **17**(2),
921 193–203, doi:10.1144/1354-0793/10-026
- 922 Zhang, K., Wu, Y., & Pruess, K. 2008. User 's Guide for TOUGH2-MP - A Massively Parallel Version of
923 the TOUGH2 Code. *Lawrence Berkeley National Laboratory Report LBNL-315E*
- 924 Zhou, Q, Birkholzer, J., Tsang, C. & Rutqvist, J. 2008. A method for quick assessment of CO₂ storage
925 capacity in closed and semi-closed saline formations. *International Journal of Greenhouse Gas*
926 *Control*, **2**(4), 626–639, doi:10.1016/j.ijggc.2008.02.004
- 927 Zhou, Quanlin, Birkholzer, J. T., Mehnert, E., Lin, Y.-F. & Zhang, K. 2010. Modeling basin- and plume-
928 scale processes of CO₂ storage for full-scale deployment. *Ground water*, **48**(4), 494–514,
929 doi:10.1111/j.1745-6584.2009.00657.x
- 930